



Star Clusters in the Elliptical Galaxy NGC 4589 Hosting a Calcium-rich SN Ib (SN 2005cz)

Myung Gyoon Lee¹ , In Sung Jang² , and Jisu Kang¹

¹ Astronomy Program, Department of Physics and Astronomy, Seoul National University, Gwanak-gu, Seoul 151-742, Republic of Korea; mglee@astro.snu.ac.kr

² Leibniz-Institut für Astrophysik Potsdam (AIP), An der Sternwarte 16, D-14482, Potsdam, Germany

Received 2018 April 1; revised 2018 December 2; accepted 2018 December 4; published 2019 January 21

Abstract

NGC 4589, a bright E2 merger-remnant galaxy, hosts the peculiar fast and faint calcium-rich SN Ib SN 2005cz. The progenitor of Ca-rich SNe Ib has been controversial: it could be (1) a young, massive star with $6\text{--}12 M_{\odot}$ in a binary system, or (2) an old, low-mass star in a binary system that was kicked out from the galaxy center. Moreover, previous distance estimates for this galaxy have shown a large spread, ranging from 20 to 60 Mpc. Thus, using archival *Hubble Space Telescope*/ACS *F435W*, *F555W*, and *F814W* images, we search for star clusters in NGC 4589 in order to help resolve these issues. We find a small population of young star clusters with $25 < V \leq 27$ ($-7.1 < M_V \leq -5.1$) mag and age < 1 Gyr in the central region at $R < 0.5$ (< 3.8 kpc), thus supporting the massive-star progenitor scenario for SN 2005cz. In addition to young star clusters, we also find a large population of old globular clusters. In contrast to previous results in the literature, we find that the color distribution of the globular clusters is clearly bimodal. The turnover (Vega) magnitude in the *V*-band luminosity functions of the blue (metal-poor) globular clusters is determined to be $V_0(\text{max}) = 24.40 \pm 0.10$ mag. We derive the total number of globular clusters, $N_{\text{GC}} = 640 \pm 50$, and the specific frequency, $S_N = 1.7 \pm 0.2$. Adopting a calibration for the metal-poor globular clusters, $M_V(\text{max}) = -7.66 \pm 0.14$ mag, we derive a distance to this galaxy: $(m - M)_0 = 32.06 \pm 0.10(\text{ran}) \pm 0.15(\text{sys})$ ($d = 25.8 \pm 2.2$ Mpc).

Key words: galaxies: distances and redshifts – galaxies: elliptical and lenticular, cD – galaxies: individual (NGC 4589) – galaxies: star clusters: general – ISM: supernova remnants

Supporting material: machine-readable table

1. Introduction

SNe Ib are the remnants of the collapsed core of massive WC Wolf–Rayet stars that lost most of their outer hydrogen envelope (so they are sometimes called thin-stripped core-collapse SNe; Smartt 2009). Their spectra show a distinguishable He I 5876 Å line but little sign of silicon lines. Recently, a new type of SN Ib called Ca-rich SNe Ib has been discovered in NGC 1032 (Perets et al. 2010). The spectra of the early phase of Ca-rich SNe Ib show He I lines, while the spectra of their late phase show Ca lines. Ca-rich SNe Ib are much fainter and show a faster decline rate in their light curves compared to normal SNe Ib (see the review by Taubenberger 2017, in his Section 5).

Ca-rich SNe Ib host many interesting properties. First, about 50% of all Ca-rich SNe Ib are found in E or S0 galaxies (Perets et al. 2010; Kasliwal et al. 2012; Taubenberger 2017). It is difficult to reconcile this fact with the conventional concept of massive stars being the progenitors of normal SNe Ib. Second, they are often found much farther from the center of their host galaxies, and they are found even in the intracluster or intragroup region, so they are sometimes called homeless SNe (Kasliwal et al. 2012; Foley 2015; Lunnan et al. 2017). Third, Lyman et al. (2016) found no evidence of globular clusters or dwarf galaxies at the position of known Ca-rich SNe in the *Hubble Space Telescope* (*HST*) images, and they concluded that the progenitors of these Ca-rich SNe must have come from somewhere else, offset from the current SN position.

These results have made the origin of Ca-rich SN Ib progenitors controversial, whether it is (1) a young, massive star with $6\text{--}12 M_{\odot}$ in a binary system (Kawabata et al. 2010; Gvaramadze et al. 2017; Moriya et al. 2017), or (2) an old, low-

mass star in a binary system that was kicked out from the galaxy center or elsewhere (Perets et al. 2011; Foley 2015; Lyman et al. 2016).

One of the most popular targets to study the progenitors of Ca-rich SNe Ib has been NGC 4589 hosting SN 2005cz (Kawabata et al. 2010; Perets et al. 2011; Foley 2015). NGC 4589 is a bright, X-ray-emitting elliptical galaxy with a LINER nucleus. It is the brightest member of a loose group of galaxies (group no. 107 in Geller & Huchra 1983). The red integrated color $((V - I) = 1.18)$ and the relatively faint *F160W*-band absolute magnitude of the surface brightness fluctuation (SBF) of NGC 4589 indicate that this galaxy is dominated by old stellar populations (Jensen et al. 2003, see their Figures 2–4). Basic properties of NGC 4589 are summarized in Table 1.

However, the distance to NGC 4589 is still uncertain. Previous distance estimates for this galaxy show a large spread (ranging from 20 to 60 Mpc), though distance estimates based on the SBF method show a much smaller spread (de Vaucouleurs & Olson 1984; Faber et al. 1989; Willick et al. 1997; Tonry et al. 2001; Jensen et al. 2003; Theureau et al. 2007; Blakeslee et al. 2010). Therefore, in this study, we estimate the distance to this galaxy using the luminosity functions of the globular clusters (GCLFs) detected in this galaxy (Harris 2001; Richtler 2003; Di Criscienzo et al. 2006; Rejkuba 2012).

More interestingly, observations of NGC 4589 show several peculiar features (Hakobyan et al. 2008). It hosts a dust disk that is aligned along the minor axis, and it is rotating fast around its major axis (Moellenhoff & Bender 1989). Ionized gas emission is detected along the minor axis at $R < 20''$ from the galaxy center. Moellenhoff & Bender (1989) found that both gas and stellar components show strong rotation with

Table 1
Basic Parameters of NGC 4589

Parameter	Value	Reference
R.A.(2000)	12 ^h 37 ^m 25 ^s .0	RC3
Decl.(2000)	74°11'31"	RC3
Type	E2, LINER	RC3
Foreground extinction, A_B , A_V , and A_I	0.102, 0.077, and 0.042	Schlafly & Finkbeiner (2011)
Distance modulus, ($m - M$) ₀	32.06 ± 0.18	GCLF, this study
Distance, d [Mpc]	25.8 ± 2.2	GCLF, this study
Image scale	125 pc arcsec ⁻¹	This study
B total magnitude, B^T	11.69 ± 0.15	RC3
V total magnitude, V^T	10.73 ± 0.15	RC3
B absolute magnitude, M_B	-20.47 ± 0.23	RC3, This study
V absolute magnitude, M_V	-21.41 ± 0.23	RC3, This study
Position angle ^a	89° (B), 92° (K)	RC3
$D_{25}(B)$	189''70 × 153''66	RC3
$D_{total}(K)$	249''00 × 186''75	Jarrett et al. (2003)
Effective radius, R_{eff}	30''4 ± 3''0 (3800 ± 400 pc)	Moellenhoff & Bender (1989)
Heliocentric velocity, v_h	1980 ± 14 km s ⁻¹	RC3

Note.

^a Position angles measured in the B and K band images, respectively.

complex kinematics. They suggested that a gas-rich galaxy fell into NGC 4589 and formed a rotating dust disk in the inner region of the galaxy, and that NGC 4589 is in an advanced state of merging. A small amount of H_2 gas, $9.1 \times 10^7 M_\odot$, was detected in this galaxy from CO observations (Sofue & Wakamatsu 1993). Polycyclic aromatic hydrocarbon (PAH) emissions at 11.3 μ m were detected in the position of the dust lanes, and far-IR and 17 μ m PAH emissions were found in the more extended regions of NGC 4589 (Kaneda et al. 2008, 2010). Kaneda et al. (2010) suggested that 11.3 μ m PAH features may be due to the gas brought in by an early merger, and the far-IR emission and 17 μ m PAH features are relics of a later merger.

If NGC 4589 had a recent wet merger, then there may be a population of young star clusters that can provide the massive-star progenitor for SN 2005cz. Motivated by this idea, we search for star clusters in NGC 4589 using *HST* images in the archive, and we investigate their properties to tell whether any young to intermediate-age clusters exist or not in this galaxy.

To date, there is only one published paper on the star clusters in NGC 4589. Kundu & Whitmore (2001) presented VI photometry of bright globular clusters with $21 < V < 24.5$ mag in NGC 4589 based on shallow *HST*/WFPC2 $F555W$ and $F814W$ images. They found no bimodality in the color distribution of these globular clusters, which is in contrast to the cases of other bright elliptical galaxies that show mostly strong bimodality (Brodie & Strader 2006; Harris et al. 2017 and references therein). This may be an intrinsic nature of NGC 4589 or due to the shallow photometry in their study. Thus, nothing is known about any of the young star clusters in this galaxy.

This paper is organized as follows. Section 2 describes how we select star clusters from the *HST* images of NGC 4589. In Section 3, we present photometric properties of the detected star clusters, as well as their spatial and radial distributions. We derive their GCLFs and use them to determine the distance to

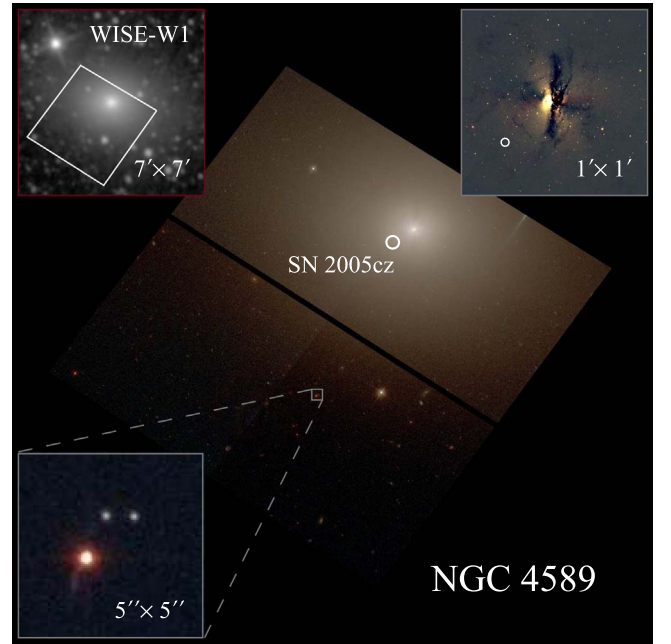


Figure 1. *HST* color images of NGC 4589 hosting SN 2005cz (circles). North is up, and east is to the left. Upper left: *WISE* W1 image for $7' \times 7'$ field. Upper right: a zoomed-in $1' \times 1'$ *HST* image of the central region from which the galaxy light model was subtracted. Lower left: a zoomed-in $5'' \times 5''$ image of a halo field shows two globular cluster candidates (two white sources).

NGC 4589. In Section 4, we discuss the origin of SN 2005cz in relation to our results, compare our GCLFs with the previous study, and compare our distance estimate with previous distance estimates. Finally we summarize the main results in the conclusion.

2. Data Reduction and Star Cluster Selection

2.1. Data

We used Advanced Camera for Surveys (ACS) images for NGC 4589 from the *HST* archive (PI: Smartt, ID: 10498). The exposure times are 1500 s for $F435W$, 1500 s for $F555W$, and 1600 s for $F814W$. We combined individual images of NGC 4589 within the same filter using AstroDrizzle (Gonzaga et al. 2012). The image scale of the combined images is 0''.05 per pixel.

Figure 1 displays a color image of the *HST* field, the location of which is marked in the *WISE*-W1 (3.6 μ m) image in the upper left. SN 2005cz is located at $\sim 13''$ (1.6 kpc for the adopted distance of 25.8 Mpc here) southeast from the galaxy center, as marked by the circle close to the galaxy center. In the upper right, we display a zoomed-in image of the central region of NGC 4589 from which the galaxy light model was subtracted. Note the presence of dust lanes that are perpendicular to the major axis (which is almost horizontal in the image) in the central region. A zoomed-in image of a southern field in the lower left shows two compact sources, which are star cluster candidates in NGC 4589 (the red bright source below is a foreground star).

2.2. Data Reduction

We reduced the data following the procedures used in the study of star clusters in Coma galaxies by Lee & Jang (2016). We derived model images of the galaxy light using IRAF/

ellipse after masking all of the bright sources except NGC 4589. Then we subtracted the model galaxy images from the drizzled images for better source detection. The resulting images are used for source detection and photometry with DAOPHOT (Stetson 1994). A master source list was made from the *F814W* image with a detection threshold of 5σ .

Effective radii of typical globular clusters are 2–3 pc, so globular clusters at the distance of NGC 4589 are expected to appear as point sources or as slightly resolved sources in the *HST*/ACS images with an image scale of ~ 6 pc per pixel. The magnitude difference between small and large apertures is one of the most effective central concentration parameters to distinguish between point sources and extended sources (Whitmore et al. 1999; Peng et al. 2011), as shown in the study of star clusters using the *HST* images for Coma galaxies in Lee & Jang (2016). We calculated the values of the *F814W* magnitude concentration parameter for the detected sources using aperture magnitudes with radii of 1.5 pixels and 3.0 pixels, $C(1.5 \text{ pix} - 3.0 \text{ pix})$.

We derived *F814W* aperture correction values for the sources including star cluster candidates following the method used in Lee & Jang (2016). The steps are as follows. First, we selected isolated bright sources with a varying range of concentration parameters. For these selected sources, we calculated the value of the magnitude difference between the aperture radii of 10 and 4 pixels, $\Delta(10 \text{ pix} - 4 \text{ pix})$. From linear fitting, we obtain $\Delta(10 \text{ pix} - 4 \text{ pix}) = -0.564C(1.5 \text{ pix} - 3.0 \text{ pix}) + 0.175$ with $\text{rms} = 0.028$. We applied this aperture correction to derive a magnitude for the aperture radius of 10 pixels ($= 0''.5$). Then we derived *F435W* and *F555W* magnitudes from *F814W* magnitudes using the 4 pixel radius colors of the sources, for example, $F555W(10 \text{ pix}) = F814W(4 \text{ pix}) + \Delta(10 \text{ pix} - 4 \text{ pix}) + (F555W - F814W)(4 \text{ pix})$. Finally, we applied a further aperture correction for radii $= 0''.5$ to infinity using the values provided by the STScI (-0.106 mag for *F435W*, -0.096 mag for *F555W*, and -0.098 mag for *F814W*).

If we use aperture corrections for radii $= 4$ – 10 pixels derived for each band and apply them to obtain their colors, the resulting colors will have larger errors. The method adopted in this study is valid only if there is no color gradient in the 4 – 10 pixel region of the sources.

According to the enclosed energy distribution of point sources in the ACS data listed in Table 3 of Sirianni et al. (2005), the stellar fluxes within a certain radius have a slight variation depending on the filter. The fractions of stellar flux within a 4 pixel radii aperture in this table are 0.832, 0.843, and 0.833 for *F435W*, *F555W*, and *F814W*, respectively. These flux variations lead to very small color differences: $\Delta(F435W - F555W) = +0.014 \text{ mag}$ ($= -2.5 \times \log_{10}(0.832/0.843)$), and $\Delta(F555W - F814W) = -0.013 \text{ mag}$ ($= -2.5 \times \log_{10}(0.843/0.833)$). We ignored this small color correction before deriving the total magnitudes of the *F555W* and *F814W* bands.

The instrumental magnitudes in the *HST* system were converted to the standard calibrated *BVI* magnitudes in the Johnson–Cousins system using the information in Sirianni et al. (2005). The photometric zero points (c_0) and color terms (c_1) we used are as follows: $c_0 = 25.842$ and $c_1 = -0.089$ for *F435W*, $c_0 = 25.704$ and $c_1 = -0.054$ for *F555W*, and $c_0 = 25.495$ and $c_1 = -0.002$ for *F814W*. Transformation uncertainties are estimated to be $\pm 0.02 \text{ mag}$ in each band.

However, we noted that the photometric zero points for ACS/WFC have a slight dependence on time. The photometric transformation in Sirianni et al. (2005) was made using *HST*

data for NGC 2419 and 47 Tuc taken in 2002, but observations for NGC 4589 were obtained in 2006. According to the STScI web page,³ the photometric zero points for *F435W*, *F555W*, and *F814W* in 2006 are on average 0.03 mag smaller than those in 2002. This variation in zero points could lead to larger systematic uncertainties in the transformation. We, therefore, adopt a conservative value of $\pm 0.03 \text{ mag}$ for the final uncertainty associated with the photometric transformation. In this study, we use Vega magnitudes and use the “0” subscripts for extinction-corrected quantities in the following analysis.

2.3. Size Estimation

We estimated the effective radii of bright sources with $V \leq 25$ using the ISHAPE program (Larsen 1999). A point-spread function (PSF) modeling is one of the most important steps in the ISHAPE run. In *HST* data, synthetic PSFs (e.g., TinyTim PSFs; Krist et al. 2011) are optimized for individual frame images. Individual frame images (*_flc.fits) have a strong geometric distortion, so using synthetic PSFs may not be the best choice (see the ISHAPE manual for details). For this reason, many previous studies used drizzled images, which are geometric-distortion-corrected and mostly coadded images, with empirical PSFs. However, modeling empirical PSFs is not always easy. Most extragalactic *HST* fields have a limited number of isolated bright stars, and they have a stellar spectral energy distribution (SED) different from target star clusters. Selecting a clean point source is also not easy because of the presence of blended stars, compact star clusters, and compact background galaxies. All of these difficulties are possible sources of uncertainties in the size estimation.

Thus we adopted an alternative approach to solving most of the problems mentioned above by using TinyTim PSFs with a single-drizzled image. The steps are as follows. We generated 400 TinyTim PSFs and placed them onto chip 1 (science extension 4) and chip 2 (science extension 1) of an flc image. We set a spectral type of K4V for the PSFs, similar to those of old globular clusters. We then drizzled this single-frame flc image. The output image is corrected for the geometric distortion but is not coadded. This image was used for generating the input PSFs using IRAF/DAOPHOT for the ISHAPE run. The drizzled images we used for the aperture photometry are coadded, so they are not ideal for size estimation based on the modeled PSFs.

We prepared *F814W*-band single-drizzled images (from one flc image) of the original NGC 4589 data and used them for size estimation. We used a King model with a concentration parameter of 30 to fit sources. The mean size for each stellar object was computed from individual frame measurements with a median-based σ -clip algorithm set at 2σ . We assigned the standard deviation of the clipped size values for size estimation errors. Angular radii were converted to linear radii, adopting a distance of 25.8 Mpc as derived in the following section.

2.4. Star Cluster Selection

Before selecting star cluster candidates in the list of the detected sources, we visually inspected the images of all detected sources with $V(\text{total}) \leq 27 \text{ mag}$ and removed artifacts, blended sources, and sources with irregular morphology. We set this magnitude limit by considering the photometric depth

³ <http://www.stsci.edu/hst/acs/analysis/>

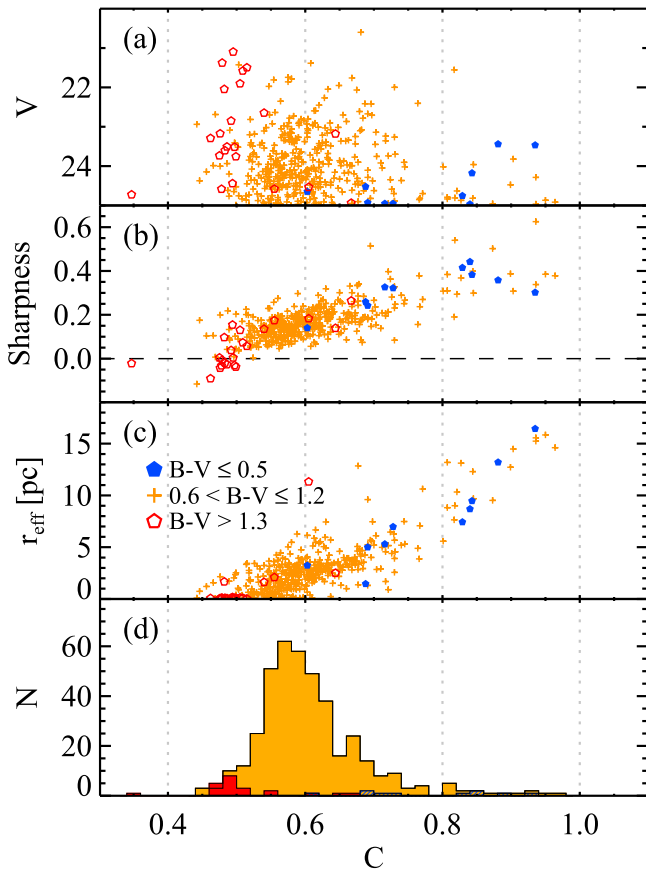


Figure 2. Characteristics of the magnitude concentration parameter C (1.5 pix–3.0 pix) for the clean sample of the sources with $V \leq 25$ mag selected through visual inspection (452 sources out of 546 sources): (a) V magnitudes, (b) DAOPHOT sharpness parameters, (c) ISHAPE effective radii, and (d) the number distribution of C for the bright sources. Blue, orange, and red symbols represent the blue ($B - V \leq 0.5$), yellow ($0.6 < (B - V) \leq 1.2$), and red ($(B - V) > 1.3$) sources, respectively. The bright red sources show a strong concentration at $C \approx 0.5$, indicating that they are mostly stars. Note that the entire sample is dominated by the orange sources, and they show a strong peak at $C \approx 0.6$. They are mostly star clusters in NGC 4589. The blue sources are much fainter than the others, and they have, on average, a larger value of C than the other groups. They are mostly background galaxies.

needed to cover a much fainter magnitude than the peak of the GCLF and the capacity of our visual inspection. Visual inspection of the images becomes difficult for the fainter sources. We selected 745 out of 2973 inspected sources. This is the star cluster search sample.

We prepared another sample that includes only bright sources with $V \leq 25$ mag. We selected 452 out of 546 inspected sources with $V \leq 25$ mag. The sources in the bright sample have smaller photometric errors and are better for analysis than the fainter sources. We use this bright sample for the following analysis of structural parameters and colors of the sources.

Figure 2(a) displays V -band magnitudes versus C for the selected bright sources with $V \leq 25$ mag. We divided the detected sources according to their color: the blue sources with $(B - V) \leq 0.5$, the globular cluster-like sources with $0.6 < (B - V) \leq 1.2$, and the red sources with $(B - V) > 1.3$. We adopted the color intervals for globular cluster selection based on the color distributions of Milky Way globular clusters (Harris 1996). We chose our color selection intervals for the blue and red sources to have the cleanest and least-contaminated sample

of blue sources and red sources. Figures 2(b) and (c) display, respectively, the DAOPHOT sharpness parameter values and effective radii versus C . In Figure 2(d), we plotted the C number distributions for these sources.

Several features are noted in Figure 2. First, there is a strong concentration of sources at $C \approx 0.5$ – 0.7 . They are dominated by sources with globular cluster-like colors. Most of these sources are slightly resolved sources. Thus these sources are mostly globular clusters in NGC 4589. The median value of the effective radii of the globular clusters in NGC 4589 in this study is 2.5 pc (rms = 1.7 pc), which is similar to the value for the Milky Way globular clusters, 3 pc (Harris 1996). Second, the red sources show a narrow vertical plume at $C \approx 0.5$ in Figure 2(a). The sources with $C \approx 0.5$ have a median DAOPHOT sharpness value of 0.004 (rms = 0.072), which shows that they are point sources. These point sources are dominated by red dwarf stars in the Milky Way. Third, the number of blue sources is small. Blue sources show a broad distribution of C , and most of them have, on average, much larger C values and fainter magnitudes than the other two groups. They are considered to be mostly background galaxies. Fourth, the values of sharpness and effective radii show a strong correlation with the values of C . This shows that C is a very effective parameter to distinguish point sources and extended sources.

We select, as the initial star cluster candidates, the slightly extended sources with $0.52 < C \leq 0.8$ (referred to as the compact sources hereafter) and the point sources with $C \leq 0.52$. The C distribution of the red sources, which are mostly foreground stars, shows a peak at $C \approx 0.5$ and declines to a zero value at $C > 0.52$. On the other hand, the C distribution of the globular cluster-like sources shows a peak at $C \approx 0.6$ and declines to a zero value at $C > 0.8$. Therefore we chose $0.52 < C \leq 0.8$ to have the cleanest and least-contaminated GC sample. The selected cluster candidates are composed of mainly slightly resolved star clusters and a small number of point sources. The selected point sources are considered to be mostly unresolved star clusters or stars.

In Table 2 we present a catalog of the star clusters in NGC 4589, including their BVI photometry and effective radii.

2.5. Completeness Tests

We estimated the completeness of our photometry using artificial sources. We generated images of the star cluster-like sources with $0.55 < C \leq 0.65$. We assumed that the luminosity function of the sources is Gaussian with a peak at a V -band total magnitude of 24.5 mag and a width of 1.0 mag, similar to the luminosity function of the globular clusters in NGC 4589 derived in the following section. We adopted four colors for the artificial sources: $(B - V) = 0.2$ and 1.4 ($(V - I) = 0.7$ and 1.4), which are close to the mean colors of the young and very red star clusters, and $(B - V) = 0.75$ and 0.95 ($(V - I) = 1.0$ and 1.2), which are close to the mean colors of the blue and red globular clusters.

We injected 250 artificial clusters onto the original image to create a test image. We repeated this procedure 1000 times and prepared 1000 test images. We set the artificial sources to have a centrally concentrated spatial distribution. The central region at $R < 0.1$ is masked out. We analyzed these test images using the same procedures as used for the original images in order to estimate the recovery rates, that is, the ratios of the number of recovered sources with respect to the number of input sources.

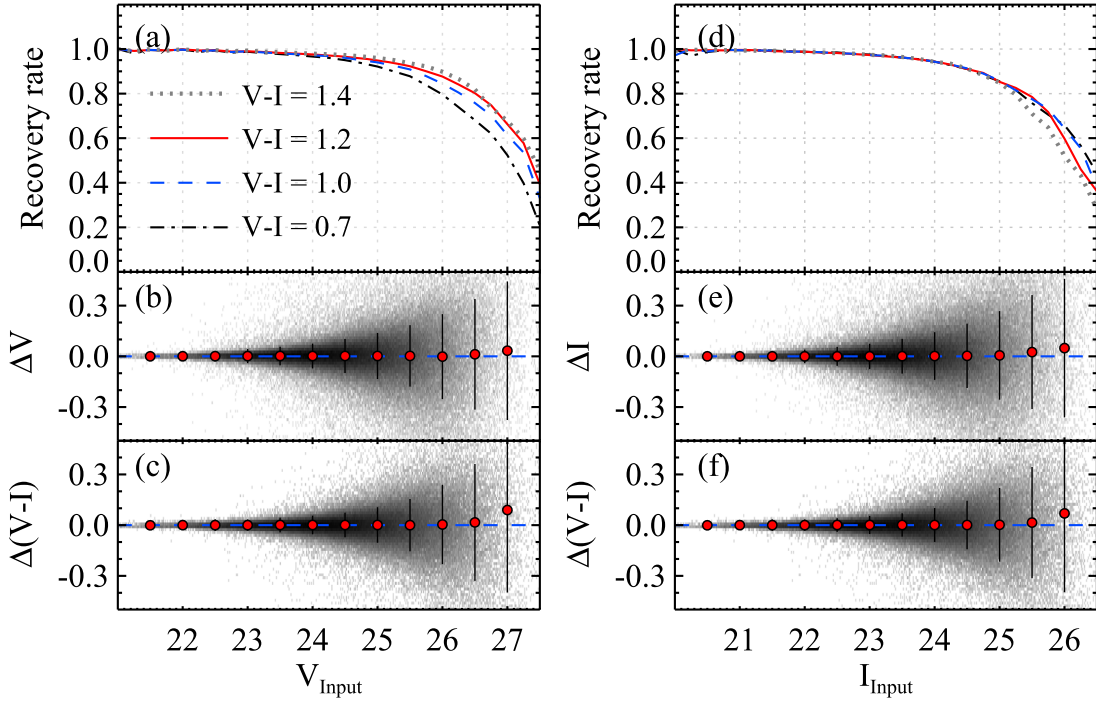


Figure 3. Results of the completeness tests for the V (left panels) and I (right panels) bands. Recovery rates (top panels), input magnitudes minus output magnitudes (middle panels), and input colors minus output colors (bottom panels) versus magnitudes. Lines in the top panels are for $(V-I) = 0.7, 1.0, 1.2$, and 1.4 ($(B-V) = 0.2, 0.75, 0.95$, and 1.4), respectively. Red circles with error bars in the middle and bottom panels denote the mean values with $\pm 1\sigma$ for given magnitudes. The input sources have a magnitude range of $21 < V < 28$ mag (corresponding to $20 < I < 27$ mag for $(V-I) = 1.0$).

Table 2
BVI Photometric Catalog of the Star Clusters with $V \leq 27$ mag in NGC 4589

ID	R.A. (J2000)	Decl. (J2000)	V (mag)	$\text{err}(V)$	$(B-V)$	$\text{err}(B-V)$	$(V-I)$	$\text{err}(V-I)$	r_{eff} (pc)	$\text{err}(r_{\text{eff}})$ (pc)	C_I^a	Remarks ^b
1	189.530546	74.171445	26.002	0.194	1.100	0.350	0.802	0.162	0.705	...
2	189.523901	74.168912	26.014	0.134	0.560	0.191	1.332	0.119	0.691	...
3	189.519277	74.169479	23.733	0.018	1.394	0.046	2.227	0.017	0.02	0.05	0.475	...
4	189.518752	74.178858	24.658	0.050	0.748	0.069	0.942	0.041	0.65	1.05	0.603	GC
5	189.513980	74.171037	25.916	0.198	0.067	0.141	0.256	0.143	0.705	...

Notes.

^a Concentration parameters derived from the F814W image.

^b Globular cluster candidates are marked by “GC.”

(This table is available in its entirety in machine-readable form.)

Figure 3 displays the results of the artificial source experiments. The recovery rates for $V = 27$ mag are 52%, 61%, 66%, and 68% for $(V-I) = 0.7, 1.0, 1.2$, and 1.4 , respectively. The mean values of the input magnitudes minus the output magnitudes are smaller than 0.03 mag for $V \leq 26.5$ mag and $I \leq 25.5$ mag.

In Figure 4 we plot the V -band 50% completeness level as a function of galactocentric distance. The 50% recovery magnitudes become fainter as galactocentric distance increases. For $(V-I) = 1.0$, the 50% recovery magnitude is $V = 26.2$ mag at $R = 0'.3$, $V = 27.3$ mag at $R = 0'.9$, and $V \approx 27.5$ at $R = 1'.3$ – $2'.6$.

3. Results

3.1. Color–Magnitude Diagrams of the Star Clusters

We display the color–magnitude diagrams (CMDs) of the point sources ($C \leq 0.52$), the compact sources ($0.52 < C \leq 0.8$), and the extended sources ($0.8 < C \leq 1.0$) with $V \leq 27$ mag in Figure 5. The error bars in the left side represent

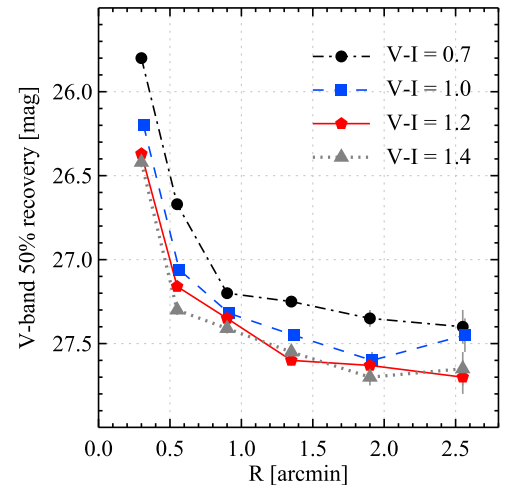


Figure 4. The 50% completeness level as a function of the galactocentric distance. Circles, squares, pentagons, and triangles are for $(V-I) = 0.7, 1.0, 1.2$, and 1.4 , respectively. The central region at $R < 0'.1$ was masked out.

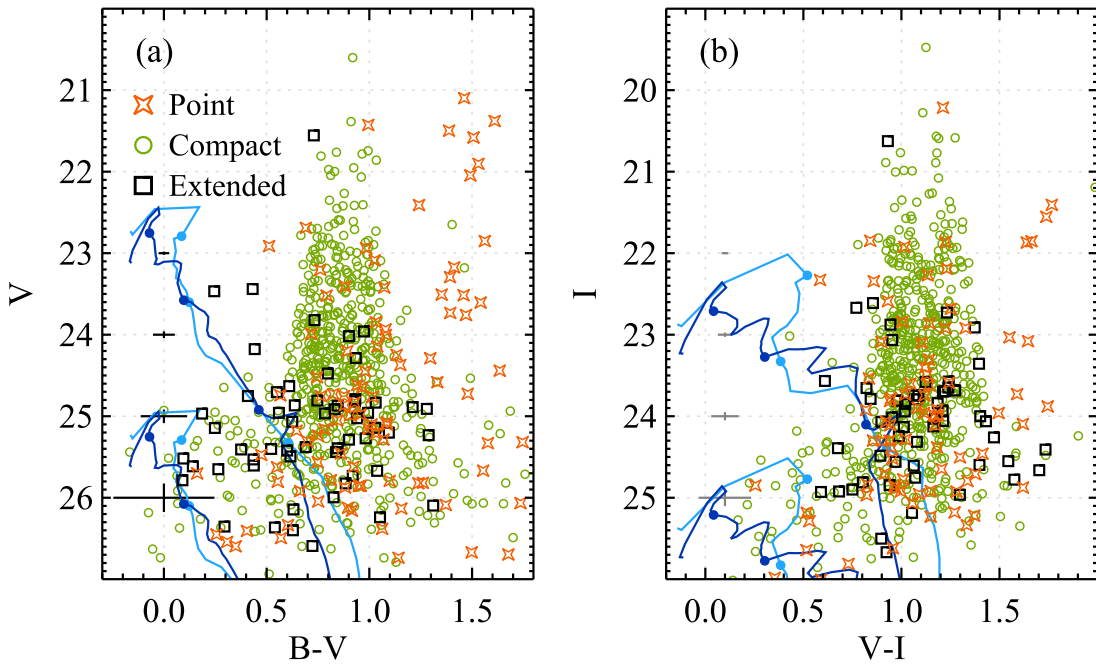


Figure 5. $V - (B - V)$ (left panel) and $I - (V - I)$ (right panel) CMDs of the selected sources with $C \leq 1$ and $V \leq 27$ mag in NGC 4589: the point sources with $C \leq 0.52$ (orange stars), the compact sources with $0.52 < C \leq 0.8$ (green circles), and the extended sources with $0.8 < C \leq 1.0$ (black boxes). The point and compact sources with $0.6 < (B - V) \leq 1.2$ ($0.8 < (V - I) \leq 1.4$) in the vertical plume are mostly globular clusters in NGC 4589. The very red point sources at $1.3 < (B - V) \leq 1.6$ ($1.5 < (V - I) \leq 1.8$) are mostly dwarf stars in the Milky Way. The extended sources are mostly background galaxies. The mean photometric errors for a given magnitude of all the detected sources are plotted. Padova SSP models with solar (cyan lines) and 0.1 solar (blue lines) metallicities are overlotted. Upper and lower SSP lines indicate masses $M_{\text{SC}} = 10^{4.5}$ and $10^{3.5} M_{\odot}$. Ages for 10^7 , 10^8 , and 10^9 yr are marked by solid circles on the SSP models.

median photometric errors for given magnitudes derived from the photometry of all the measured sources. We also plotted Padova simple stellar population (SSP) models for solar metallicity (cyan lines) and $0.1 Z_{\odot}$ (blue lines) with cluster mass $M/M_{\odot} = 10^{3.5}$ and $10^{4.5}$ (Girardi et al. 2000).

These CMDs show several notable features. First, the most distinguishable feature is a broad vertical branch at $0.6 < (B - V) \leq 1.2$ ($0.8 < (V - I) \leq 1.4$), the brightest of which reaches $V \approx 21$ mag ($I \approx 20$ mag). This branch consists of a dominant population of compact sources and a small number of point sources. The colors of these sources are similar to those of typical globular clusters. Thus the sources in this branch are mostly considered to be globular clusters in NGC 4589. The branch also contains a small population of extended objects whose colors are numerically not much different from those of the globular clusters. They are mostly background galaxies.

Second, there is a small population of blue compact sources at $(B - V) \leq 0.5$ ($(V - I) \leq 0.7$), which are bluer than the blue limit for the globular clusters. They are mostly fainter than $V = 25$ mag ($I = 24$ mag), so they are much fainter than the majority of the globular clusters. These sources can be either young star clusters in NGC 4589 or background galaxies. To investigate their nature further, we inspect their spatial and radial distributions in the following sections.

Third, there is a narrow vertical sequence of very red point sources with $21 < V \leq 25$ mag at $1.3 < (B - V) \leq 1.6$. They have $(V - I)$ colors of 1.5–3.0, as seen in Figure 6, and many of them present in the $(B - V)$ panel are outside the plotted range for the $(V - I)$ plot. They are mainly red dwarf stars in the Milky Way.

Fourth, extended sources show a much broader color distribution and fainter magnitudes compared with compact

sources. The number of extended sources is much smaller than that of compact sources, and the spatial distribution of extended sources appears to be uniform.

3.2. Color-Color Diagrams of the Star Clusters

Figure 6 shows the color-color diagram of the point sources, the compact sources, and the extended sources. The left and right panels display the sources with $V \leq 25$ mag ($M_V \leq -7.1$ mag) and those with $V \leq 27$ mag ($M_V \leq -5.1$ mag), respectively. We also plotted Padova evolutionary tracks for the SSPs with solar metallicity (cyan lines) and $0.1 Z_{\odot}$ (blue lines) and the 12 Gyr isochrones for $[\text{Fe}/\text{H}] = -2.3$ to $+0.0$ (red lines). The solid circles along the evolutionary track represent the age, 10^7 , 10^8 , 10^9 , and 10^{10} yr. In this diagram, the globular clusters are located along the 12 Gyr isochrones for a large range of metallicities, showing that they are indeed old globular clusters with a large range of metallicities.

The blue sources with $(B - V) \leq 0.5$ (and $(V - I) < 1.0$) are located around the SSP models with age < 1 Gyr, but with a large scatter. The mean photometric errors of these blue sources are $\text{err}(B - V) = 0.13$ ($\text{err}(V - I) = 0.12$) for $25 < V \leq 26$ mag and $\text{err}(B - V) = 0.25$ ($\text{err}(V - I) = 0.21$) for $26.0 < V \leq 27$ mag. Therefore, the large scatter in color is mainly due to photometric errors.

There are a small number of extended sources that overlap the color-color sequence of globular clusters. One of the extended sources has $V = 21.6$ mag, as bright as the brightest globular clusters, and the rest are more than two magnitudes fainter than this. The effective radius of the brightest extended source is 7.6 pc, smaller than the values for ultracompact dwarfs (UCDs), so it is considered to be an extended bright globular cluster. Thus none of them are found to be UCDs.

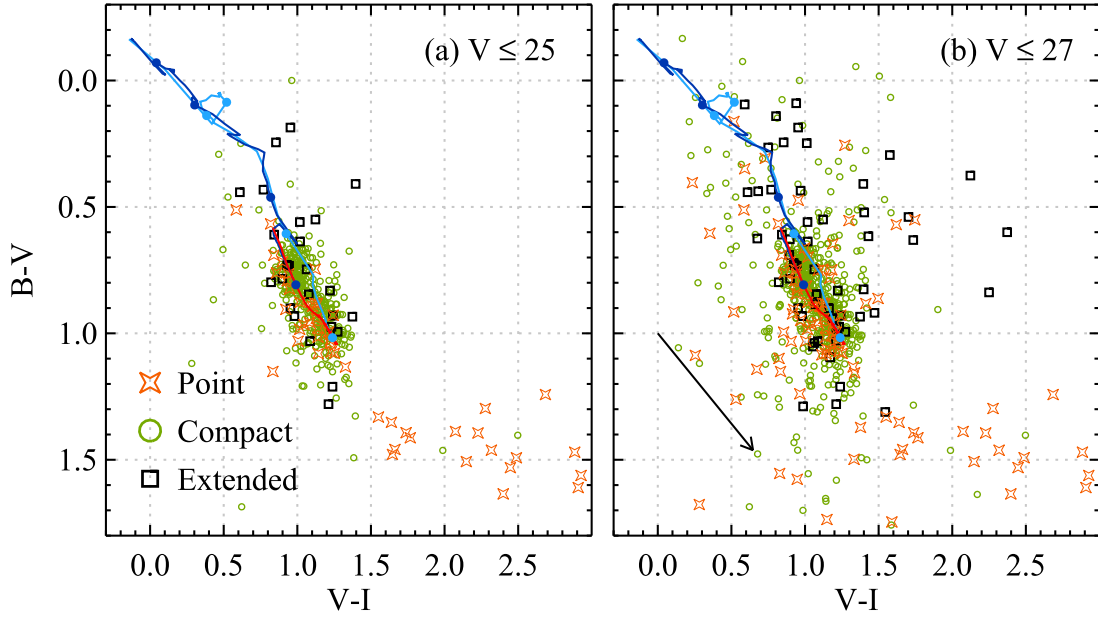


Figure 6. Color-color diagrams of the selected sources with $V \leq 25$ mag (a) and $V \leq 27$ mag (b) in NGC 4589. A Padova SSP model for 12 Gyr and $[\text{Fe}/\text{H}] = -2.3$ to 0.2 is overplotted by a red solid line in each panel. Two lines indicate SSP models with solar (cyan) and 0.1 solar (blue) metallicities. Solid circles mark $\log(\text{age} [\text{yr}]) = 7, 8, 9, \text{ and } 10$. The point and compact sources in the strong concentration area at $0.6 < (B - V) \leq 1.2$ and $0.8 < (V - I) \leq 1.4$ are mostly globular clusters in NGC 4589. The reddening vector is marked by an arrow.

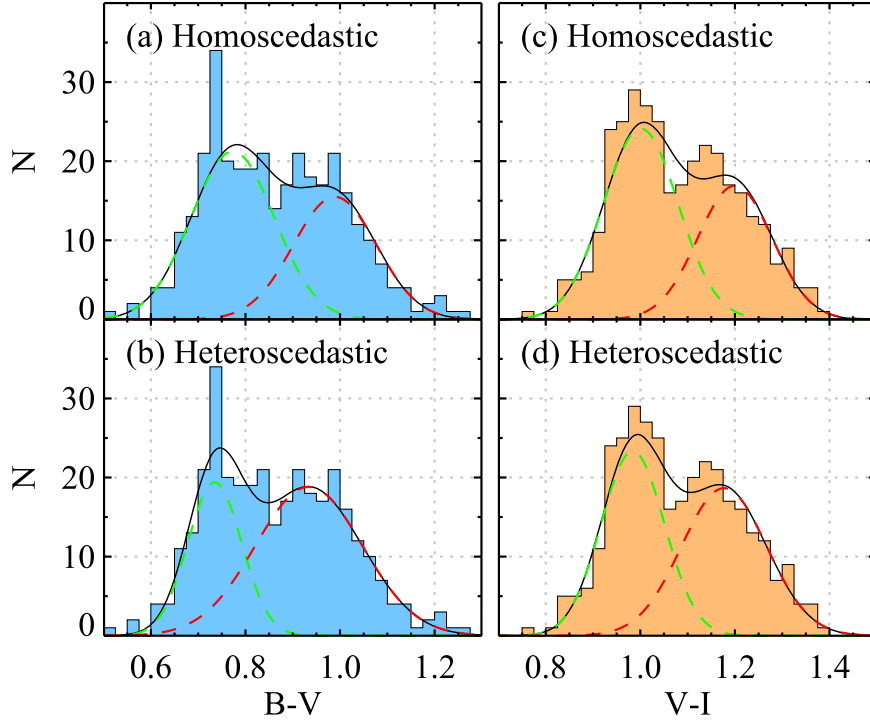


Figure 7. $(B - V)$ (a, b) and $(V - I)$ (c, d) color distributions of the globular cluster candidates ($C \leq 0.8$) with $V \leq 25$ mag at $0.2 < R < 2'$ in NGC 4589 for the same variance and the varying variance, respectively. The sources with $0.6 < (B - V) \leq 1.2$ ($0.8 < (V - I) \leq 1.4$) are mostly globular clusters in NGC 4589. Solid curved lines denote the fitting with GMM, and green and red dashed lines are the Gaussian components for blue GCs and red GCs, respectively.

3.3. Color Distributions of the Globular Clusters

Figure 7 shows the color distributions of the bright star cluster candidates with $C \leq 0.8$ and $V \leq 25$ mag at $0.2 < R < 2'$ in NGC 4589. The most prominent feature in this figure is due to globular clusters in NGC 4589. The color distributions of these globular clusters show two peaks in both $(B - V)$ and $(V - I)$ colors, clearly suggesting that they are bimodal, as often seen in other early-type galaxies.

We applied a Gaussian mixture modeling (GMM) test (Muratov & Gnedin 2010) to this sample. We chose an option for the same variance (homoscedastic case) as well as the varying variance (heteroscedastic case). The results of this test are summarized in Table 3. Key parameters from this test are the probability for a unimodal distribution (p), the ratio of the separation of the two peak colors relative to their widths (D), and the kurtosis k . If D is larger than two, the distribution is

Table 3
Summary of GMM Tests for Color Distributions of the GCs with $V \leq 25$ mag in NGC 4589

	Color	Blue GCs			Red GCs			D^a	p^a	k^a
		Mean	σ	N_{total}	Mean	σ	N_{total}			
Homoscedastic ^b	$(B - V)$	0.78 ± 0.01	0.09 ± 0.01	200 ± 21	0.99 ± 0.02	0.09 ± 0.01	138 ± 21	2.38 ± 0.28	$1.94e-4$	-0.493
	$(V - I)$	1.00 ± 0.01	0.08 ± 0.01	201 ± 14	1.20 ± 0.01	0.08 ± 0.01	137 ± 14	2.60 ± 0.20	$3.93e-6$	-0.702
Heteroscedastic ^c	$(B - V)$	0.73 ± 0.01	0.06 ± 0.02	107 ± 39	0.93 ± 0.03	0.12 ± 0.02	231 ± 39	2.06 ± 0.38	$1.37e-5$	-0.493
	$(V - I)$	0.99 ± 0.02	0.07 ± 0.01	174 ± 33	1.18 ± 0.02	0.09 ± 0.01	164 ± 40	2.50 ± 0.24	$2.94e-5$	-0.702

Notes.

^a D represents the ratio of the separation of the two peak colors relative to their widths, p denotes the probability for a unimodal distribution, and k is the kurtosis.

^b Same variances for the Gaussian fits.

^c Varying variances for the Gaussian fits.

considered to be bimodal. A negative value for k is necessary for bimodal distributions.

In Table 3 the values of p are close to zero ($< 10^{-3}$), and the values of D are larger than two for all cases. The values of k are smaller than zero in all cases. Thus, these results show that the color distributions are indeed bimodal. The blue and red peaks are found to be at $(B - V) = 0.78 \pm 0.01$ and 0.99 ± 0.02 ($(V - I) = 1.00 \pm 0.01$ and 1.20 ± 0.01) for the homoscedastic case, and at $(B - V) = 0.73 \pm 0.01$ and 0.93 ± 0.03 ($(V - I) = 0.99 \pm 0.02$ and 1.18 ± 0.02) for the heteroscedastic case. In the case of the homoscedastic option, the number ratio of the blue GCs and the red GCs derived from the $(B - V)$ colors (200 versus 138) is similar to the value from the $(V - I)$ colors (201 versus 137). However, in the case of the heteroscedastic option, the number ratio of the blue GCs and the red GCs derived from the $(B - V)$ colors (107 versus 231) is significantly different from the value based on the $(V - I)$ colors (174 versus 164). Therefore, the results for the homoscedastic option appear to be more reliable.

In summary, we select, as the globular clusters, the compact and point sources ($C \leq 0.8$) with globular cluster-like colors of $0.6 < (B - V) \leq 1.2$. For the following analysis, we divided the globular cluster sample into two subgroups according to their color: blue (metal-poor) globular clusters with $0.6 < (B - V) \leq 0.85$ and red (metal-rich) globular clusters with $0.85 < (B - V) \leq 1.2$. We chose, as the division colors, the colors with a minimum value between the two peaks in the color histograms.

Blue globular clusters in the brightest cluster galaxies (BCGs) often show a color–magnitude relation known as the blue tilt (see Harris et al. 2006, 2017 and references therein). In Figure 8, we display the $I - (B - I)$ CMD of the globular clusters in NGC 4589 to check the presence of any blue tilt. We divided the bright globular clusters with $21 < I \leq 24$ mag into five groups according to their I -band magnitudes in steps of $\Delta I = 0.5$ mag. We set the brightest magnitude bin to sample all the globular clusters with $21 < I \leq 22$ mag. The number of globular clusters in these groups ranges from 46 ($21 < I \leq 22$ mag) to 108 ($23.0 < I \leq 23.5$ mag).

We measured the mean colors of the blue and red globular clusters in each group using the GMM code. The measured values of D were larger than two in all groups, but the values of p were not always close to zero ($< 10^{-5}$). This indicates that the unimodal distribution is not always rejected, although the bimodal distribution is meaningful in all cases. The same-variance and varying-variance options in the code yield similar

colors for the faint bins ($I < 22.5$ mag), but slightly different values for the brighter bins ($I > 22.5$ mag). The difference in the brighter bins is due to the smaller sample size compared to that of the fainter bins.

Fitting the bright blue globular clusters with $21 < I \leq 23$ ($-11.1 < M_I \leq -9.1$) mag, we obtained the values of the slope γ_I ($21 < I \leq 23$) = $d(B - I)/dI = -0.034 \pm 0.036$ for the homoscedastic option and γ_I ($21 < I \leq 23$) = -0.095 ± 0.044 for the heteroscedastic option. If we extend the magnitude range down to $I = 24$ ($M_I = -8.1$) mag, we obtain the slope values γ_I ($21 < I \leq 24$) = -0.012 ± 0.017 and -0.009 ± 0.019 for the homoscedastic and heteroscedastic options, respectively. Thus, the slope value for the bright globular cluster sample ($21 < I \leq 23$ mag) derived with the heteroscedastic option shows a hint of blue tilt at the level of 2σ , while the values for the other cases do not.

Harris et al. (2006) presented an $M_I - (B - I)_0$ CMD for the combined sample of globular clusters in eight BCGs (their Figure 21), which shows clearly a blue tilt for $-11.8 < M_I < -9.5$ mag. They provided only a mass (M)–metallicity (Z) relation derived from the CMDs, $Z \propto M^{0.55}$, and did not present the value of the blue tilt slope in the CMD. We estimate the value of the slope for the blue tilt in their Figure 21, obtaining $\gamma_I \approx -0.09$. Thus the slope value for the bright globular cluster sample ($21 < I \leq 23$ mag) of NGC 4589 derived with the heteroscedastic option in this study, $\gamma_I = -0.095 \pm 0.044$, is similar to the mean slope for the BCGs in Harris et al. (2006). Recently, Harris et al. (2017) presented an $M_{F814W} - (F475W - F814W)_0$ CMD for the combined sample of globular clusters in five other BCGs (see their Figure 22), and they pointed out that the estimated slopes of the blue tilt show a large spread among galaxies, which range from $\gamma_M = d \log Z / d \log M \sim 0$ to $+0.27$ (or $\gamma_I = d(F475W - F814W) / dF814W \sim 0$ to -0.05). These values are much smaller than that given in Harris et al. (2006), $\gamma_M = 0.55$.

3.4. Spatial Distributions of the Star Clusters

In Figure 9 we plotted the spatial distributions of the point and compact sources with $V \leq 25$ mag (left panels) and $25 < V \leq 27$ mag (right panels): (a) and (e) all sources, (b) and (f) blue sources ($(B - V) \leq 0.5$, bluer than the globular clusters), (c) and (g) blue globular clusters ($0.6 < (B - V) \leq 0.85$) and red globular clusters ($0.85 < (B - V) \leq 1.2$), and (d) and (h) red sources ($1.5 < (B - V) \leq 1.8$), redder than the

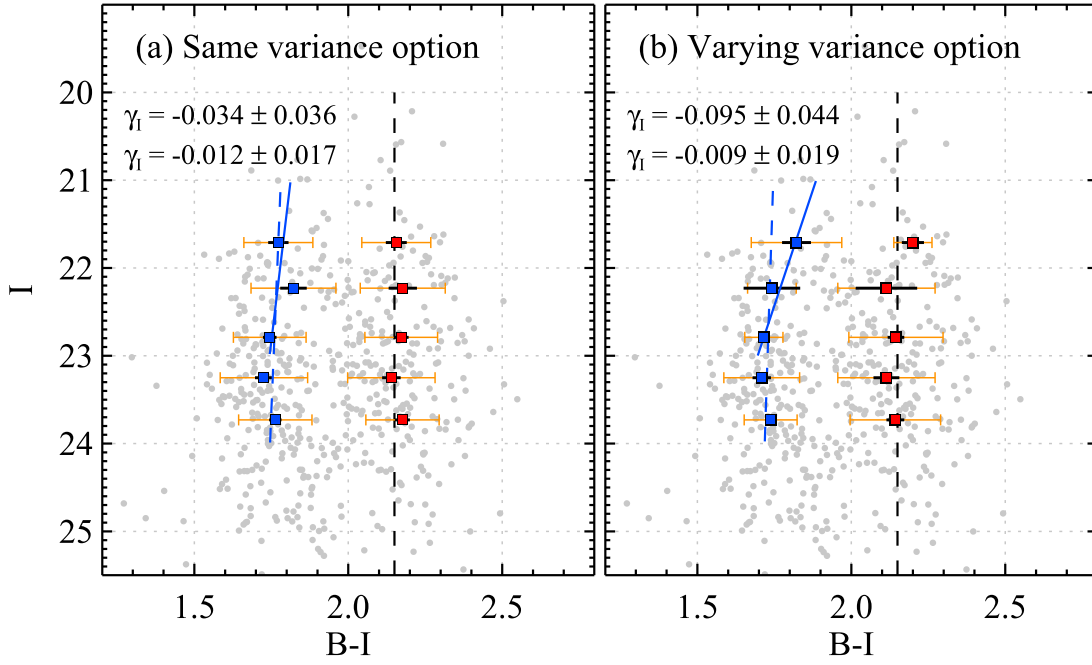


Figure 8. $I - (B - I)$ CMDs of the globular cluster candidates ($C \leq 0.8$ and $0.6 < B - V \leq 1.2$) in NGC 4589. The mean colors of the blue and red subpopulations were measured using the GMM code with two options: a same-variance option (a) and a varying-variance option (b). Yellow and black error bars indicate the sigmas and errors of the mean colors. The solid and dashed lines represent linear fits for the blue subpopulations with $21 < I \leq 23$ mag and $21 < I \leq 24$ mag. Measured values of the slopes are given in each panel. The approximate mean color for the red subpopulation is shown by the vertical dashed line.

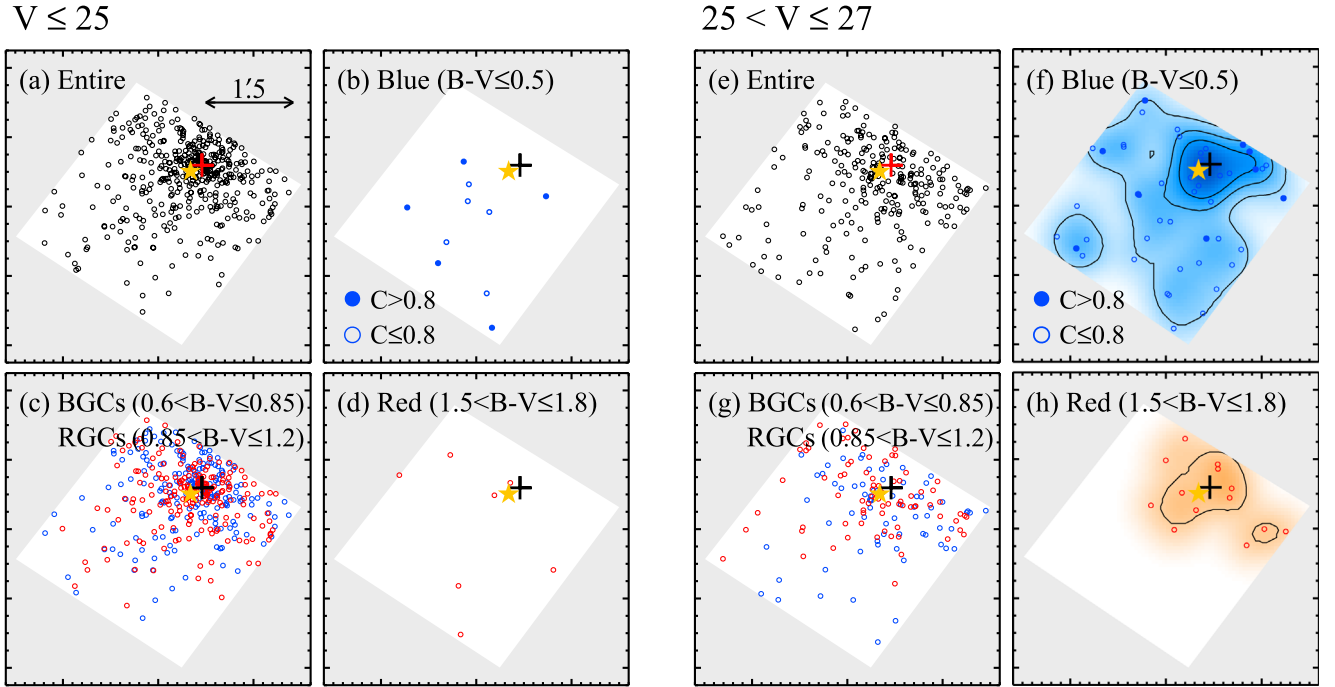


Figure 9. Spatial distributions of the selected point and compact sources ($C \leq 0.8$) with $V \leq 25$ mag (left) and $25 < V \leq 27$ mag (right) in NGC 4589: (a), (e) all sources, (b), (f) blue sources ($(B - V) \leq 0.5$), (c), (g) blue GCs and red GCs ($0.60 < (B - V) \leq 0.85$ and $0.85 < (B - V) \leq 1.20$), (d), (h) red sources ($1.5 < (B - V) \leq 1.8$). In (b) and (f) we also plotted the extended blue sources ($C > 0.8$) for comparison. Contours in (f) and (h) represent the number density map of the blue sources and the red sources with $25 < V \leq 27$ mag. The locations of the galaxy center and SN are marked by the cross and the yellow star.

globular clusters. In Figures 9(b) and (f), we also plotted the spatial distributions of the extended blue sources with $C > 0.8$ with solid circles in order to check their membership. The spatial distributions of these extended sources do not show any central concentration, which indicates that they are background galaxies. We also marked the positions of the galaxy center (cross) and SN 2005cz (yellow star) in the figure.

A few interesting features are noted in this figure. First, the spatial distributions of both blue and red globular clusters in Figures 9(c) and (g) show a strong central concentration around the galaxy center. This result implies that these sources are indeed globular clusters that are gravitationally bound to NGC 4589.

Second, the spatial distribution of the bright red sources (with $V \leq 25$ mag) in Figure 9(d) is roughly uniform, which

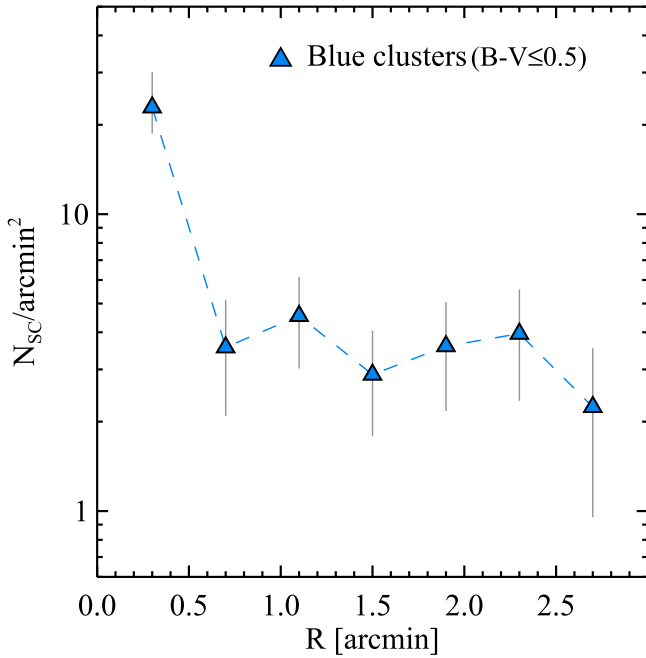


Figure 10. Completeness-corrected radial number density profile for the blue ($B - V \leq 0.5$) sources with $V \leq 27.0$ mag in NGC 4589. The central region at $R < 0.1$ is masked out. Note that the blue sources show a clear central excess at $R \lesssim 0.5$, which indicates that they are young star clusters in NGC 4589.

indicates that they are not the members of NGC 4589. Considering that the majority of these sources are point sources, we conclude that they are red dwarf stars in the Milky Way.

Third, the number-density contour maps in Figure 9(f) indicate that the spatial distribution of the faint blue sources appears to show a weak central concentration around the galaxy center. The nature of the faint blue sources will be checked further with their radial number density profile in the following section.

Fourth, the number-density contour map in Figure 9(h) indicates that the spatial distribution of the faint red sources appears to show a very weak central concentration around the galaxy center, but the number of sources is too small to be significant. In this figure, we plotted the red sources $1.5 < (B - V) \leq 1.8$ to avoid any contamination from the faint red globular clusters.

3.5. Radial Distributions of the Young Star Clusters

To further investigate the nature of the blue sources seen in the CMDs, we selected the blue sources with $C \leq 0.8$, $(B - V) \leq 0.5$, and $V \leq 27.0$ mag. The number of these blue sources is 46. Then we derived their radial number density profile, as plotted in Figure 10. The errors for the number density are Poisson errors.

In deriving the radial density profiles, we excluded the central region at $R < 0.1$, which masked out most of the dust lane. We also excluded out-of-the-edge/gap regions. We calculated the true area by counting individual “pixels,” which were used for the calculation of cluster properties. Pixels around saturated stars, background galaxies, and masked regions were not used. We corrected the incompleteness of our photometry using the completeness test results as a function of galactocentric distance.

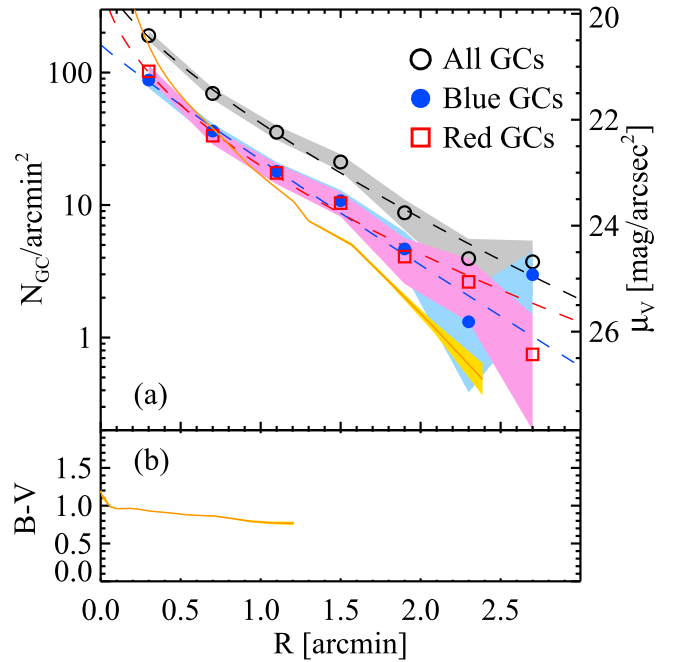


Figure 11. (a) Radial number density profiles of all GCs (black open circles), blue GCs (solid circles), and red GCs (red squares) with $V \leq 25.0$ mag in NGC 4589. Shaded regions represent the errors for the number density. The yellow solid line represents the V-band surface brightness profile of NGC 4589. Its magnitude scale is indicated in the right vertical axis. Dashed lines denote the Sérsic profile fitting to the data for all GCs ($n_{AGC} = 1.41 \pm 0.34$), blue GCs ($n_{BGC} = 1.07 \pm 0.28$), and red GCs ($n_{RGC} = 1.89 \pm 0.83$). (b) Radial profile of the $(B - V)$ color of the galaxy light.

The radial profile of the blue sources clearly shows a central excess at $R < 0.5$ (~ 3.8 kpc) and a flattening at the level of $\Sigma \approx 3 \text{ arcmin}^{-2}$ in the outer region at $R > 0.5$. This result shows that the blue sources in the central region at $R < 0.5$ are mainly the members of NGC 4589, while those in the outer region at $R > 0.5$ are most likely background galaxies. Considering as well that they are mostly compact (slightly resolved) sources, we conclude that the blue sources in the central region are mainly genuine young star clusters in this galaxy.

We estimate the background level for the blue sources using the region at $R > 1'$, and we obtain $\Sigma = 3.0 \pm 1.3 \text{ arcmin}^{-2}$. Subtracting the background level, we derive the total number of young star clusters with $24.5 < V \leq 27$ at $R < 0.5$ and obtain $N_{YSC} = 16 \pm 6$. From the comparison of these sources with the SSP models for solar metallicity and $Z > 0.1 Z_{\odot}$ (Girardi et al. 2000) as shown in Figure 5, we estimate their ages to be 10 Myr to 1 Gyr and their stellar masses to be $M = 10^{3.5}$ to $10^{4.5} M_{\odot}$. These values change little even if we use the SSP models for $Z > 0.1 Z_{\odot}$.

3.6. Radial Distributions of the Globular Clusters

We derived the radial number density profiles of the bright globular clusters with $V \leq 25$ mag in NGC 4589: all globular clusters, the blue globular clusters, and the red globular clusters. We corrected the radial profiles for the incompleteness using the results from the artificial source test.

Since the *HST* field is not large enough to cover the background region, it is difficult to estimate the background level. Therefore, we present the results without background

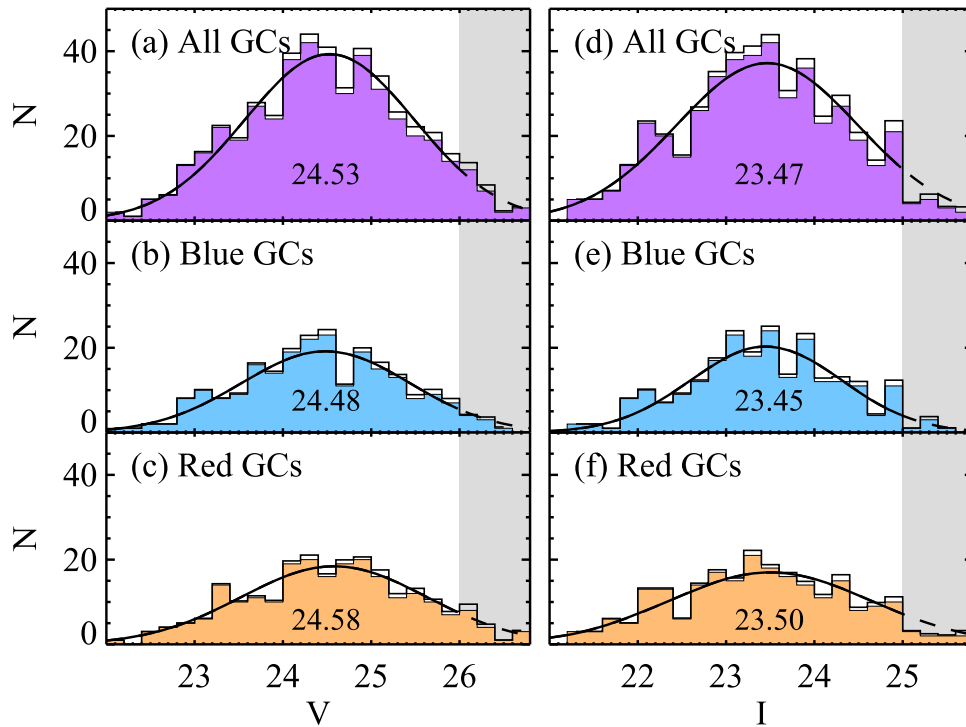


Figure 12. V-band (left) and I-band (right) luminosity functions of all GCs, blue GCs, and red GCs at $0.2 < R \leq 2'$ of NGC 4589. Solid and blank histograms represent the luminosity functions before and after completeness correction. Solid lines represent the Gaussian function fitting to the completeness-corrected data for $V \leq 26.0$ mag and $I \leq 25.0$ mag. The numbers in each panel denote the turnover magnitudes.

correction. The results for the outer region at $R > 2'$ are uncertain. Figure 11(a) displays the radial number density profiles of these globular clusters.

Fitting the profiles for $R \leq 2.5$ with a Sérsic law (Sérsic 1963), we obtain the Sérsic index values, $n_{\text{AGC}} = 1.41 \pm 0.34$ for all globular clusters, $n_{\text{BGC}} = 1.07 \pm 0.28$ for the blue globular clusters, and $n_{\text{RGC}} = 1.89 \pm 0.83$ for the red globular clusters. These values are similar to those of NGC 4921 (Lee & Jang 2016). The corresponding effective radii of the globular cluster systems are $R_{\text{eff,AGC}} = 0.94 \pm 0.09$, $R_{\text{eff,BGC}} = 0.90 \pm 0.08$, and $R_{\text{eff,RGC}} = 1.00 \pm 0.22$, respectively. Although the Sérsic index value for the blue globular clusters is slightly smaller than that for the red globular clusters, the difference is within errors. In most massive galaxies, the blue globular clusters have a shallower density profile than the red globular clusters (Lee et al. 1998; Brodie & Strader 2006, and references therein; see also Cho et al. 2016; Lee & Jang 2016; Harris et al. 2017). Therefore, NGC 4589 is a rare example that shows both blue and red subpopulations that have similar radial profiles.

For comparison, we also plotted the V-band radial surface-brightness profile, μ_V , of the galaxy light derived from the F555W image using the IRAF/ellipse task. We estimated the background levels using the area at $R > 2.5$ and used them for background subtraction.

We converted the unit for the surface brightness profile of the galaxy light, the magnitude per square arcsec, into $\log(\text{flux per square arcmin})$. In the figure we plotted $\mu_V/2.5$ for direct comparison with the radial number density profiles of globular clusters. We shifted the resulting radial profile of the galaxy light along the vertical direction to match the radial number density profile of the blue and red globular clusters at $R \sim 0.7$. In the right vertical axis we labeled the scale for the surface brightness profile.

Sérsic law fitting for the galaxy light with $0.1 < R < 2.0$ gives a Sérsic index of $n_{\text{galaxy}} = 3.11 \pm 0.21$ (with $R_{\text{eff,galaxy light}} = 0.47 \pm 0.01$), showing that the galaxy light follows the de Vaucouleurs law. The radial profile of all globular clusters is flatter than the surface brightness profile of the galaxy light, and the effective radius of the entire globular cluster system ($R_{\text{eff,AGC}} = 0.94 \pm 0.09$) is two times larger than the value for the galaxy light ($R_{\text{eff,galaxy light}} = 0.47 \pm 0.01$). This shows that the globular cluster system is more extended than the galaxy light, which is also seen in many other galaxies (see Brodie & Strader 2006 and references therein).

In Figure 11(b) we plot the radial variation of the $(B - V)$ color of the galaxy light. The color of the galaxy light is redder than $(B - V) = 1.0$ in the central region at $R \leq 0.1$ and becomes slowly bluer from $(B - V) = 1.0$ at $R = 0.1$ to $(B - V) = 0.8$ at $R = 1.2$. As shown in the color-color diagram (Figure 6), SSP models show that an old stellar population with $-2.3 < [\text{Fe}/\text{H}] < +0.2$ can have $(B - V)$ colors ranging from 0.6 to 1.1 mag. Thus, the integrated color of the galaxy light is consistent with colors of the old stellar populations with a large range of metallicities.

3.7. Luminosity Functions of the Globular Clusters

We derived V-band and I-band GCLFs for NGC 4589 by counting the number of globular clusters at $0.2 < R \leq 2.0$. We excluded the central region at $R < 0.2$, where the completeness is much lower than the outer region. We corrected the GCLFs for the completeness using the results of the completeness test. In Figure 12 we display V- and I-band GCLFs: for all globular clusters (top panels), the blue globular clusters (middle panels), and the red globular clusters (bottom panels). The GCLFs in the figure appear to be approximately

Table 4
Summary of Gaussian Fits for LF of All GCs, Blue GCs, and Red GCs in NGC 4589

	<i>V</i>			<i>I</i>		
	Center	Width	N_{total}^a	Center	Width	N_{total}^a
All GCs, $0/2 < R \leq 2'$	24.53 ± 0.06	0.96 ± 0.05	472 ± 25	23.47 ± 0.07	1.03 ± 0.07	478 ± 26
Blue GCs	24.48 ± 0.09	0.96 ± 0.07	230 ± 17	23.45 ± 0.07	0.86 ± 0.06	218 ± 16
Red GCs	24.58 ± 0.10	1.05 ± 0.10	242 ± 19	23.50 ± 0.12	1.14 ± 0.12	243 ± 21

Note.

^a The errors for the numbers are from the fitting errors for the integration of Gaussian functions provided by IDL/mpfitexpr.

Gaussian, showing a turnover (peak) at $V \approx 24.5$ mag ($I \approx 23.5$ mag).

We fit the GCLFs with a Gaussian function for the magnitude range $V \leq 26.0$ mag ($I \leq 25.0$ mag), where incompleteness of our photometry is not significant. We obtain the values of the turnover magnitudes and widths as summarized in Table 4. The turnover magnitudes and widths for all globular clusters are $V(\text{max}) = 24.53 \pm 0.06$ mag with $\sigma = 0.96 \pm 0.05$ and $I(\text{max}) = 23.47 \pm 0.07$ mag with $\sigma = 1.03 \pm 0.07$.

It is noted that the widths of the GCLFs for NGC 4589 are smaller than the value for Milky Way globular clusters, $\sigma = 1.2$ – 1.4 for the *V* band (Di Criscienzo et al. 2006; Rejkuba 2012), and those for other elliptical galaxies, $\sigma \approx 1.3$, in Kundu & Whitmore (2001). Kundu & Whitmore (2001) could not determine the value of the width for NGC 4589 because of the shallow photometric limit. However, the values in this study are similar to those for NGC 4921, the brightest spiral galaxy in Coma, $\sigma = 1.0$ – 1.1 for the *V* and *I* bands based on deep *HST* images (Lee & Jang 2016). We note that the data in this study go much deeper than that in Kundu & Whitmore (2001) and that the size of the globular cluster sample in NGC 4589 is much larger than the size of the Milky Way globular cluster sample.

Jordán et al. (2007) derived a relation between the *g*- and *z*-band GCLF width and the absolute *B*-band magnitude of their host galaxies from the ACSVCS sample: $\sigma_g = (1.14 \pm 0.01) - (0.100 \pm 0.007)(M_{B,\text{gal}} + 20)$ (similar results, but for $M_{z,\text{gal}}$, were given later for the combined sample of ACSVCS and ACSFCS by Villegas et al. 2010). If we use this relation for the luminosity of NGC 4589 ($M_B = -20.47 \pm 0.23$ mag), we obtain a value of $\sigma_g = 1.19$. The scatter of this relation for the magnitude range of NGC 4589 in Figure 9 of Jordán et al. (2007) is estimated to be about ± 0.1 . Thus the GCLF width of NGC 4589 in this study is ~ 0.2 smaller than the value expected from Jordán et al. (2007) at the level of 2σ .

The *V*-band turnover magnitude for the blue globular clusters ($V(\text{max}) = 24.48 \pm 0.09$ mag) is 0.10 mag brighter than that for the red globular clusters ($V(\text{max}) = 24.58 \pm 0.10$ mag). However, this difference is at the level of 1σ , so it is not significant. On the other hand, the *I*-band turnover magnitude for the blue globular clusters ($I(\text{max}) = 23.45 \pm 0.07$ mag) is nearly the same as the value for the red globular clusters ($I(\text{max}) = 23.50 \pm 0.12$ mag). The widths for the blue globular clusters and the red globular clusters are found to be similar.

3.8. Total Number and Specific Frequency of Globular Clusters

We estimate the total number of globular clusters in NGC 4589 using the radial number density profile and luminosity

function of the globular clusters and keeping the area coverage of the *HST*/ACS field in mind. We counted the number of blue and red globular clusters brighter than $V = 25$ mag in $R \leq 0/94 \pm 0.09$, which is the half number radius of all globular clusters we measured from the radial number density profile. It is not easy to estimate the foreground or background contamination in this value when considering the limit of the *HST* field. However, the globular cluster density is moderately high inside the half number radius of the globular cluster system, so the contribution of the foreground or background sources must not be significant. Assuming a Gaussian luminosity distribution of the globular clusters with a peak at $V = 24.53 \pm 0.06$ mag and a width of 0.96 ± 0.05 , we obtain the total number of globular clusters in NGC 4589 to be $N(\text{total}) = 640 \pm 50$. The error is derived from individual measurement errors associated with the half number radius and the luminosity distribution of the globular clusters. From this number and the absolute magnitude of NGC 4589 ($M_V = -21.41 \pm 0.23$ mag), we estimate the specific frequency and obtain $S_N = 1.7 \pm 0.2$. This value is similar to the mean value for bright E galaxies with luminosities similar to that of NGC 4589 (Harris et al. 2013).

3.9. GCLF Turnover Magnitude Calibration

We estimate the distance to NGC 4589 using the GCLF method as applied to the case of Coma galaxies in Lee & Jang (2016). The turnover magnitude of the GCLFs has been used as a standard candle for a long time (Harris 2001; Richtler 2003; Di Criscienzo et al. 2006; Rejkuba 2012). It is known that the *V*-band turnover magnitudes of the metal-poor globular clusters are brighter than or equal to those of the metal-rich globular clusters, and that this magnitude difference between the two subpopulations shows a large spread among galaxy samples (Di Criscienzo et al. 2006; Rejkuba 2012).

In an extensive review of the GCLF method, Rejkuba (2012) concluded that the luminosity functions of the metal-poor (blue) globular clusters are a better distance indicator than those using the entire sample of globular clusters because they show smaller scatter and because they are independent of the fraction of metal-rich globular clusters, which varies depending on the galaxy. Therefore we use the luminosity functions of the blue globular clusters to estimate the distance to NGC 4589.

We adopt the calibration of the *V*-band turnover magnitudes for the metal-poor globular clusters given by Di Criscienzo et al. (2006). For the zero-point calibration of the $M_V(\text{RR})$ – $[\text{Fe}/\text{H}]$ relation to be used for distance estimation of the globular clusters, Di Criscienzo et al. (2006) adopted a distance to the LMC, $(m - M)_0 = 18.50$. This value is close to the recent geometric measurement based on eclipsing binaries of the LMC (Pietrzyński et al. 2013), $(m - M)_0 = 18.494 \pm 0.008(\text{ran}) \pm$

Table 5
Summary of GCLF Distance Estimation for NGC 4589

Parameter	Value	Remarks
Systematic errors of the GCLF method		
M_V (max) (metal-poor GC)	-7.66 ± 0.09^a	Di Criscienzo et al. (2006)
Zero-point error of M_V –[Fe/H](RR) relation	$\pm 0.05^b$	Di Criscienzo et al. (2006)
Adopted error for metal-poor GC calibration of M_V (max)	$\pm 0.10^c$	This study
Intrinsic uncertainty of the turnover magnitudes (metal-poor GC)	$\pm 0.1^d$	This study
Total systematic error of the GCLF method based on metal-poor GCs	$\pm 0.14^e$	This study
NGC 4589		
Foreground extinction, A_V	0.077 ± 0.04	Schlafly & Finkbeiner (2011)
V (max) (blue GC)	24.48 ± 0.09	This study
V (max) ₀ (blue GC)	24.40 ± 0.10	after extinction correction
Aperture correction error	± 0.03	This study
Transformation error	± 0.03	Sirianni et al. (2005)
Total systematic error of the distance modulus	$\pm 0.15^f$	This study
Distance modulus, $(m - M)_0$	32.06 ± 0.18	± 0.10 (ran) ± 0.15 (sys)
Distance, d [Mpc]	25.8 ± 2.2	± 1.2 (ran) ± 1.8 (sys)

Notes.

^a Based on the samples of the metal-poor globular clusters in the Milky Way, M31, and 14 early-type galaxies (Di Criscienzo et al. 2006). The error denotes the mean error of the GCLF turnover magnitudes for the three samples of calibrator galaxies.

^b The error of the zero point for the $M_V(RR)$ –[Fe/H] relations used in Di Criscienzo et al. (2006).

^c The sum of the mean calibration error and the error for the $M_V(RR)$ –[Fe/H] relations.

^d Note that the intrinsic uncertainty of the turnover magnitudes based on the entire globular clusters is ± 0.2 mag (Richtler 2003; Rejkuba 2012).

^e The sum of the calibration error of M_V (max) and intrinsic uncertainty of the turnover magnitudes of the metal-poor globular clusters.

^f The sum of the aperture correction and transformation errors for NGC 4589 and the total systematic error of the GCLF method based on metal-poor globular clusters.

0.048(sys). A better calibration of the GCLF with updated data for the GCLF and the distance to their host galaxies is needed in the future. Di Criscienzo et al. (2006) derived a calibration from the selected sample of 74 metal-poor ([Fe/H] < −1.0) globular clusters located in the outer region at $2 < R_{GC} < 35$ kpc with relatively lower reddening values with $E(B - V) < 1.0$ in the Milky Way. In the Milky Way, we can observe globular clusters that are even located close to the galaxy center in addition to the halo globular clusters, but we can only observe mostly halo globular clusters in other galaxies. Therefore, the sample of globular clusters we observe in other galaxies is mostly made up of halo globular clusters, and it is closer to the sample of MW halo globular clusters, rather than to the entire sample of MW globular clusters. From this sample, Di Criscienzo et al. (2006) obtained $M_{V,MWG}$ (max) = -7.66 ± 0.11 mag. Then they derived similar calibrations from the samples of the metal-poor globular clusters in M31 and a set of 14 early-type galaxies in the literature: $M_{V,M31}$ (max) = -7.65 ± 0.19 mag and $M_{V,ETG}$ (max) = -7.67 ± 0.23 mag. These three values are in excellent agreement, but they are derived from galaxies with a wide range of morphological types, luminosity, and mass. Di Criscienzo et al. (2006) suggested, as a final calibration for the metal-poor globular clusters, a weighted mean of these three values, M_V (max) = -7.66 ± 0.09 mag.

The error of the zero point for the $M_V(RR)$ –[Fe/H] relations adopted for the calibration of the turnover magnitudes in Di Criscienzo et al. (2006) is ± 0.05 mag. Combining this zero-point error and the mean error of the M_V (max) calibration, we estimate the systematic error for the metal-poor globular cluster calibration of M_V (max) to be ± 0.10 mag.

There is another source for the systematic error of the GCLF method, which is an intrinsic uncertainty (scatter) of the turnover magnitudes of the GCLFs. In the review of the GCLF method,

Rejkuba (2012; M. Rejkuba 2018, private communication) discussed several factors for the errors of the GCLF methods that use the entire globular cluster sample in a galaxy, which include environmental effects, dependence on the properties of their host galaxies, and metallicity difference between the calibrator sample and the target sample. She suggested that the turnover magnitudes of the GCLF vary from galaxy to galaxy at the level of ± 0.2 mag because the intrinsic dispersion of the turnover magnitudes depends on the sampled globular cluster system in a galaxy. Therefore, the systematic error for galaxy-to-galaxy GCLF turnover magnitude scatter due to population and sampling effects is estimated to be ± 0.2 mag in the case of the turnover magnitude measurements based on the entire globular clusters in a galaxy.

If we use only the metal-poor globular clusters, the corresponding uncertainty will be much smaller than the error based on the entire globular cluster samples because the metal-poor globular cluster calibrations based on three different samples of galaxies in Di Criscienzo et al. (2006) agree at the level of 0.01 mag. It is difficult to estimate a precise value of this error at the moment. In this study we adopt the error, in a conservative manner, to be ± 0.1 mag.

Combining this error due to the intrinsic scatter (± 0.1) and the systematic error of the M_V (max) calibration (± 0.10), we estimate the total systematic error for the GCLF distance estimation to be ± 0.14 mag in the case of the metal-poor globular cluster samples. The corresponding error will be ± 0.22 mag in the case of the entire globular cluster samples. We summarize these errors in Table 5.

3.10. GCLF Distance Estimation for NGC 4589

Applying the adopted V-band calibration for the metal-poor globular clusters (M_V (max) = -7.66 ± 0.14) to the measured

turnover magnitude ($V(\text{max}) = 24.48 \pm 0.09$ and $V(\text{max})_0 = 24.40 \pm 0.10$), we derive the distance to NGC 4589: $(m - M)_0 = 32.06 \pm 0.10(\text{ran}) \pm 0.15(\text{sys}) = 32.06 \pm 0.18$ ($d = 25.8 \pm 2.2$ Mpc). For the calculation of the errors, we included all uncertainties due to foreground extinction correction, aperture correction, and transformation uncertainties, as summarized in Table 5.

If we use this result for the calibration of the I -band magnitudes for NGC 4589 globular clusters, we obtain $M_I(\text{max}) = (23.45 \pm 0.07) - 0.042 - (32.06 \pm 0.18) = -8.65 \pm 0.19$ mag, where 0.042 is the value for the I -band foreground extinction. This value is similar to the calibration adopted in Lee & Jang (2016), $M_I(\text{max}) = -8.56 \pm 0.09$ mag.

4. Discussion

4.1. The Origin of SN 2005cz and Ca-rich SNe Ib

To explain the spectral features and the light curves of SN 2005cz, Kawabata et al. (2010) suggested that the origin of SN 2005cz is a core-collapse supernova whose progenitor is a massive star at the low-mass end ($8\text{--}12 M_\odot$) in a binary system. They noted a possible relation between SN 2005cz and the young stellar population in the nucleus of NGC 4589. From the analysis of the spectrum of the NGC 4589 nucleus, Zhang et al. (2008) suggested that the nucleus is dominated by old, low-mass stars (age $> 10^{10}$ yr and mass $M < 1 M_\odot$), with 11% of the nucleus composed of young stars (age $= 10^7\text{--}10^8$ yr and mass $M < 10 M_\odot$). Kawabata et al. (2010) pointed out that the progenitor of SN 2005cz might have come from these young stars in the nucleus.

Later, Suh et al. (2011) presented, from *GALEX* NUV and SDSS photometry, that the observed (NUV- r) color of NGC 4589 is close to the color of a galaxy that had little recent star formation (see their Figure 2). Considering the possible presence of internal extinction due to dust clouds, they inferred that the intrinsic color of NGC 4589 may be much bluer than the observed color, and they favored the massive-star origin of SN 2005cz. They suggested that the progenitor of SN 2005cz may have a mass of $5\text{--}6 M_\odot$, which is even lower than the value of $8\text{--}12 M_\odot$ suggested by Kawabata et al. (2010). However, there is no information on the estimated value of the internal extinction, so it is not possible to tell whether the observed color is intrinsically red or significantly reddened by internal dust.

In contrast, Perets et al. (2011) used optical spectroscopy, $H\alpha$ emission, *GALEX* UV emission, and *HST* images to search for any signatures of young stellar populations around SN 2005cz. In particular, they tried to find young, massive stars ($M > 15 M_\odot$) from the photometry of point sources around the SN location using *HST*/WFPC2 and ACS images. However, Perets et al. (2011) found no feature of any young stellar population either close to or far (> 1.5 kpc) from the position of SN 2005cz, supporting the old, low-mass star origin scenario of SN 2005cz. Perets et al. (2011) disfavored the massive-star origin of SN 2005cz and showed that the SED of NGC 4589 covering *GALEX* FUV to 2MASS K_s is fitted very well by an old galaxy model with an age of 12.5 Gyr, stellar mass of $10^{11.17} M_\odot$, and no specific star formation rate.

In this study, we found a small population of young star clusters in the central region at $R < 0.5$ (< 3.8 kpc) that includes the location of SN 2005cz. Most of these star clusters are slightly resolved (i.e., larger than point sources), so they cannot be

individual stars in NGC 4589. Their colors range from $(B - V) = 0$ to 0.5 ($(V - I) = 0.2$ to 0.7), which indicates that they are younger than about 10^9 yr. The magnitudes of these clusters are $25 < V \leq 27$ ($-7.1 < M_V \leq -5.1$) mag. These magnitudes correspond to the masses of $10^{3.5}\text{--}10^{4.5} M_\odot$ for the Padova SSP models with solar metallicity. The mass range does not change much with the choice of metallicity for $Z \gtrsim 0.1 Z_\odot$. These young clusters are found only in the central region at $R < 0.5$ (< 3.8 kpc), while old globular clusters are found in a much wider area with a much higher abundance. These young star clusters might have formed in relation with a recent merger that resulted in a rotating dust disk (Moellenhoff & Bender 1989). They might have provided a massive-star progenitor for SN 2005cz. Therefore, our finding of young star clusters in the central region of NGC 4589 supports the massive-star progenitor scenario for the origin of Ca-rich SNe Ib.

4.2. Comparison with the Previous GCLF

Using shallow *HST*/WFPC2 $F555W$ and $F814W$ images, Kundu & Whitmore (2001) derived a GCLF for NGC 4589 from the sample of globular clusters with $21 < V < 24.5$ mag. They could not determine the value of the GCLF width for NGC 4589 because of the shallow photometric limit. They fitted it with a Gaussian function for a fixed width of $\sigma = 1.3$. They obtained turnover magnitudes of $V(\text{max})_0 = 25.22 \pm 0.39$ and $I(\text{max})_0 = 24.21 \pm 0.41$. These values are ~ 0.8 mag fainter than those in this study, $V(\text{max})_0 = 24.45 \pm 0.07$ mag and $I(\text{max})_0 = 23.43 \pm 0.07$ mag. The turnover magnitudes in Kundu & Whitmore (2001) are about 0.9 mag fainter than the 50% completeness limits of their photometry, $V_{\text{lim}} = 24.3$ mag and $I_{\text{lim}} = 23.2$ mag. Their photometry did not reach the turnover magnitudes, and the errors of their estimated magnitudes are as large as 0.4 mag. Note that our photometry reaches much deeper than the turnover magnitudes. Therefore the differences between Kundu & Whitmore (2001) and this study are considered to be mainly due to the shallow photometry in Kundu & Whitmore (2001).

Kundu & Whitmore (2001) also presented the total number of globular clusters, $N(\text{total}) = 789 \pm 123$, and the specific frequency, $S_N = 5.1 \pm 3.7$. In this estimation, they adopted $(m - M)_0 = 31.95$ and $M_V = -21.2$ mag for NGC 4589. However, this value is a local S_N , constructed from a shallow photometry of a sample based on only a small fraction of the entire galaxy, so it cannot be compared directly with our estimate.

4.3. Comparison with Previous Distance Estimates

In Table 6, we list the previous estimates of the distance to NGC 4589 based on various methods. The distances based on the $D_n\text{--}\sigma$ relation, the Faber–Jackson relation, and the Tully–Fisher relation show a large scatter ($(m - M)_0 = 31.60$ to 33.91) and have large errors from 0.25 to 0.40 mag (de Vaucouleurs & Olson 1984; Faber et al. 1989; Willick et al. 1997; Theureau et al. 2007). The distance in this study, $(m - M)_0 = 32.06 \pm 0.18$ ($d = 25.8 \pm 2.2$ Mpc), is in the middle of these values.

In contrast, the distances based on the SBF have smaller errors than the others. Tonry et al. (2001) presented a distance of $(m - M)_0 = 31.71 \pm 0.22$ based on the I -band SBF. This value was updated to a 0.16 mag smaller value later by Jensen et al. (2003), $(m - M)_0 = 31.55 \pm 0.22$, who used the Udalski

Table 6
List of Previous Distance Estimates for NGC 4589

Method	Distance modulus (Distance)	Reference
$D_n-\sigma$	33.91 ± 0.25 (60.6 Mpc)	Faber et al. (1989)
$D_n-\sigma$	32.93 ± 0.40 (38.6 Mpc)	Willick et al. (1997)
Faber–Jackson	31.60 ± 0.39 (20.9 Mpc)	de Vaucouleurs & Olson (1984)
Tully–Fisher	32.55 ± 0.40 (32.3 Mpc)	Theureau et al. (2007)
SBF	31.71 ± 0.22 (22.6 Mpc)	Tonry et al. (2001)
SBF	31.55 ± 0.22 (20.4 Mpc)	Jensen et al. (2003), updated Tonry et al. (2001) <i>I</i> -band
SBF	31.77 ± 0.24^a (20.4 Mpc)	Blakeslee et al. (2010), updated Tonry et al. (2001) <i>I</i> -band
SBF	32.07 ± 0.13^a (25.9 Mpc)	Blakeslee et al. (2010), updated Jensen et al. (2003) <i>F160W</i> -band
GCLF	32.06 ± 0.18 (25.8 Mpc)	This study

Note.

^a The errors include the systematic ± 0.1 mag error in the optical and near-IR SBF measurements (Blakeslee et al. 2010; Cantiello et al. 2018).

et al. (1999) Cepheid period–luminosity relation for the calibration of the method. However, metallicity correction for Cepheid distances needs to be taken into account for better distance estimation. Considering this, Blakeslee et al. (2010) published a correction formula to Tonry et al. (2001) distances (see Appendix A of the paper). The appendix also contains some clarifications on the differences between the SBF distances by Tonry et al. (2001) and by Jensen et al. (2003). According to this correction, the revised distance modulus to NGC 4589 is derived to be $(m - M)_0 = 31.77 \pm 0.22$ mag.

Jensen et al. (2003) also presented near-IR SBF measurements of NGC 4589. The distance modulus to NGC 4589 based on the near-IR SBF measurements can be derived using the \bar{m}_{F160W} value in their Table 2 (column 4) and the \bar{M}_{F160W} value in their Equation (1). We derive a distance modulus $(m - M)_0 = 27.21(\pm 0.08) + 4.76(\pm 0.03) = 31.97 \pm 0.09$ mag. Following the suggestion in Blakeslee et al. (2010), we apply the correction for the metallicity-dependent Cepheid zero point of Tonry et al. (2001), 0.1 mag, to this value, and we obtain $(m - M)_0 = 32.07 \pm 0.09$.

All of the errors in the above SBF distances are random errors. The systematic error of each of the optical and near-IR SBF distances is $\sim \pm 0.1$ mag based on the Cepheid zero-point error (Jensen et al. 2003; Cantiello et al. 2018). Considering both the random errors and the systematic errors, the distance moduli based on optical and near-IR SBF measurements to NGC 4589 are $(m - M)_0$ (optical SBF) = 31.77 ± 0.24 and $(m - M)_0$ (NIR SBF) = 32.07 ± 0.13 , respectively.

Thus, the near-IR SBF distance modulus is 0.3 ± 0.3 mag larger than the optical SBF value. However, the difference is similar to its error, so both values agree at the level of 1σ . The distance in this study, $(m - M)_0 = 32.06 \pm 0.18$, is 0.3 mag larger than the revised optical SBF distance, $(m - M)_0 = 31.77 \pm 0.24$, but is in excellent agreement with the near-IR SBF distance, $(m - M)_0 = 32.07 \pm 0.13$ (Jensen et al. 2003; Blakeslee et al. 2010).

5. Summary and Conclusion




Using deep *HST*/ACS images, we detected a significant population of star clusters in NGC 4589. This population is dominated by old globular clusters, but includes a small population of young star clusters in the central region. We present *BVI* photometry of these clusters in the Vega magnitude system. The main results are summarized as follows:

1. We found a small population of young star clusters with age $< 10^9$ yr in the central region at $R < 0.5$ (< 3.8 kpc) of NGC 4589. These young clusters might have provided a massive-star progenitor for SN 2005cz, which supports the massive-star origin scenario of Ca-rich SNe Ib.
2. The color distribution of the globular clusters is clearly bimodal. GMM analysis with a homoscedastic option identifies a blue peak at $(B - V) = 0.78 \pm 0.01$ ($(V - I) = 1.00 \pm 0.01$) and a red peak at $(B - V) = 0.99 \pm 0.02$ ($(V - I) = 1.20 \pm 0.01$). With a heteroscedastic option, we find the blue and red peaks at similar colors: $(B - V) = 0.73 \pm 0.01$ ($(V - I) = 0.99 \pm 0.02$) and $(B - V) = 0.93 \pm 0.03$ ($(V - I) = 1.18 \pm 0.02$).
3. The radial number density profile of the globular clusters is flatter than the surface brightness profile of the stellar light. The former is fitted by a Sérsic law with $n_{\text{AGC}} = 1.41 \pm 0.34$, while the latter is fitted well by a Sérsic law with $n_{\text{galaxy}} = 3.11 \pm 0.21$, which is close to the de Vaucouleurs profile.
4. The GCLFs are fitted well by a Gaussian function. The *V*-band turnover magnitudes for all globular clusters, the blue globular clusters, and the red globular clusters are found to be similar: $V_{\text{AGC}}(\text{max}) = 24.53 \pm 0.06$ mag for all globular clusters, $V_{\text{BGC}}(\text{max}) = 24.48 \pm 0.09$ mag for the blue globular clusters, and $V_{\text{RGC}}(\text{max}) = 24.58 \pm 0.10$ mag for the red globular clusters. The corresponding *V*-band widths are also found to be similar: $\sigma_{\text{AGC}} = 0.96 \pm 0.05$, $\sigma_{\text{BGC}} = 0.96 \pm 0.07$, and $\sigma_{\text{RGC}} = 1.05 \pm 0.10$.
5. We derived the total number of globular clusters to be $N(\text{total}) = 640 \pm 50$ and the specific frequency to be $S_N = 1.7 \pm 0.2$.
6. Considering the calibration errors of the turnover magnitudes (± 0.1 mag) and the intrinsic variation depending on their host galaxies and environment (± 0.1 mag), we estimate the total systematic error for the GCLF distance measurement to be ± 0.14 mag in the case of the metal-poor globular cluster sample, and ± 0.22 mag in the case of the entire globular cluster sample.
7. Adopting the calibration for the metal-poor globular clusters (Di Criscienzo et al. 2006; Rejkuba 2012), we derive a distance to NGC 4589 from the turnover magnitude of the blue globular clusters: $(m - M)_0 = 32.06 \pm 0.18$ and $d = 25.8 \pm 2.2$ Mpc. The distance

modulus in this study is in excellent agreement with the near-IR SBF distance, $(m - M)_0 = 32.07 \pm 0.13$, but 0.3 mag larger than the revised optical SBF distance, $(m - M)_0 = 31.77 \pm 0.24$ (Jensen et al. 2003; Blakeslee et al. 2010).

The authors would like to thank the referee for careful and useful suggestions that helped to clarify some confusing issues such as the SBF distances and helped to improve the original manuscript. The authors are also grateful to Marina Rejkuba for clarifying the uncertainties of the GCLF distances. We thank Brian Cho for improving the English in the manuscript. This work was supported by the National Research Foundation of Korea (NRF) grant funded by the Korean Government (NRF-2017R1A2B4004632). J.K. was supported by the Global PhD Fellowship Program (NRF-2016H1A2A1907015) of the National Research Foundation.

ORCID iDs

Myung Gyoon Lee  <https://orcid.org/0000-0003-2713-6744>
In Sung Jang  <https://orcid.org/0000-0002-2502-0070>
Jisu Kang  <https://orcid.org/0000-0003-3734-1995>

References

- Blakeslee, J. P., Cantiello, M., Mei, S., et al. 2010, *ApJ*, **724**, 657
- Brodie, J. P., & Strader, J. 2006, *ARA&A*, **44**, 193
- Cantiello, M., Blakeslee, J. P., Ferrarese, L., et al. 2018, *ApJ*, **856**, 126
- Cho, H., Blakeslee, J. P., Chies-Santos, A. L., et al. 2016, *ApJ*, **822**, 95
- de Vaucouleurs, G., de Vaucouleurs, A., Corwin, H. G., Jr., et al. 1991, Third Reference Catalogue of Bright Galaxies (RC3) (New York: Springer)
- de Vaucouleurs, G., & Olson, D. W. 1984, *ApJS*, **56**, 91
- Di Criscienzo, M., Caputo, F., Marconi, M., & Musella, I. 2006, *MNRAS*, **365**, 1357
- Faber, S. M., Wegner, G., Burstein, D., et al. 1989, *ApJS*, **69**, 763
- Foley, R. J. 2015, *MNRAS*, **452**, 2463
- Geller, M. J., & Huchra, J. P. 1983, *ApJS*, **52**, 61
- Girardi, L., Bressan, A., Bertelli, G., & Chiosi, C. 2000, *A&AS*, **141**, 371
- Gonzaga, S., Hack, W., Fruchter, A., & Mack, J. (ed.) 2012, The DrizzlePac Handbook (Baltimore, MD: STScI)
- Gvaramadze, V. V., Langer, N., Fossati, L., et al. 2017, *NatAs*, **1**, 0116
- Hakobyan, A. A., Petrosian, A. R., McLean, B., et al. 2008, *A&A*, **488**, 523
- Harris, W. E. 1996, *AJ*, **112**, 1487
- Harris, W. E. 2001, in Star Clusters, Saas-Fee Advanced Course 28. Lecture Notes 1998, Swiss Society for Astrophysics and Astronomy, ed. L. Labhardt & B. Binggeli (Berlin: Springer), 223
- Harris, W. E., Ciccone, S. M., Eadie, G. M., et al. 2017, *ApJ*, **835**, 101
- Harris, W. E., Harris, G. L. H., & Alessi, M. 2013, *ApJ*, **772**, 82
- Harris, W. E., Whitmore, B. C., Karakla, D., et al. 2006, *ApJ*, **636**, 90
- Jarrett, T. H., Chester, T., Cutri, R., Schneider, S. E., & Huchra, J. P. 2003, *AJ*, **125**, 525
- Jensen, J. B., Tonry, J. L., Barris, B. J., et al. 2003, *ApJ*, **583**, 712
- Jordán, A., McLaughlin, D. E., Côté, P., et al. 2007, *ApJS*, **171**, 101
- Kaneda, H., Onaka, T., Sakon, I., et al. 2010, *ApJL*, **716**, L161
- Kaneda, H., Suzuki, T., Onaka, T., Okada, Y., & Sakon, I. 2008, *PASJ*, **60**, S467
- Kasliwal, M. M., Kulkarni, S. R., Gal-Yam, A., et al. 2012, *ApJ*, **755**, 161
- Kawabata, K. S., Maeda, K., Nomoto, K., et al. 2010, *Natur*, **465**, 326
- Krist, J. E., Hook, R. N., & Stoeck, F. 2011, *Proc. SPIE*, **8127**, 81270J
- Kundu, A., & Whitmore, B. C. 2001, *AJ*, **121**, 2950
- Larsen, S. S. 1999, *A&AS*, **139**, 393
- Lee, M. G., & Jang, I. S. 2016, *ApJ*, **819**, 77
- Lee, M. G., Kim, E., & Geisler, D. 1998, *AJ*, **115**, 947
- Lunnan, R., Kasliwal, M. M., Cao, Y., et al. 2017, *ApJ*, **836**, 60
- Lyman, J. D., Levan, A. J., James, P. A., et al. 2016, *MNRAS*, **458**, 1768
- Moellenhoff, C., & Bender, R. 1989, *A&A*, **214**, 61
- Moriya, T. J., Mazzali, P. A., Tominaga, N., et al. 2017, *MNRAS*, **466**, 2085
- Muratov, A. L., & Gnedin, O. Y. 2010, *ApJ*, **718**, 1266
- Peng, E. W., Ferguson, H. C., Goudfrooij, P., et al. 2011, *ApJ*, **730**, 23
- Perets, H. B., Gal-yam, A., Crockett, R. M., et al. 2011, *ApJL*, **728**, L36
- Perets, H. B., Gal-Yam, A., Mazzali, P. A., et al. 2010, *Natur*, **465**, 322
- Pietrzyński, G., Graczyk, D., Gieren, W., et al. 2013, *Natur*, **495**, 76
- Rejkuba, M. 2012, *Ap&SS*, **341**, 195
- Richtler, T. 2003, in Stellar Candles for the Extragalactic Distance Scale, Vol. 635, ed. D. Alloin & W. Gieren (Berlin: Springer), 281
- Schlafly, E. F., & Finkbeiner, D. P. 2011, *ApJ*, **737**, 103
- Sérsic, J. L. 1963, *BAAA*, **6**, 41
- Sirianni, M., Jee, M. J., Benítez, N., et al. 2005, *PASP*, **117**, 1049
- Smartt, S. J. 2009, *ARA&A*, **47**, 63
- Sofue, Y., & Wakamatsu, K.-I. 1993, *PASJ*, **45**, 529
- Stetson, P. B. 1994, *PASP*, **106**, 250
- Suh, H., Yoon, S.-c., Jeong, H., & Yi, S. K. 2011, *ApJ*, **730**, 110
- Taubenberger, S. 2017, Handbook of Supernovae (Cham: Springer International)
- Theureau, G., Hanski, M. O., Coudreau, N., Hallet, N., & Martin, J.-M. 2007, *A&A*, **465**, 71
- Tonry, J. L., Dressler, A., Blakeslee, J. P., et al. 2001, *ApJ*, **546**, 681
- Tully, R. B., Courtois, H. M., Dolphin, A. E., et al. 2013, *AJ*, **146**, 86
- Udalski, A., Szymanski, M., Kubiak, M., et al. 1999, *AcA*, **49**, 201
- Villegas, D., Jordán, A., Peng, E. W., et al. 2010, *ApJ*, **717**, 603
- Whitmore, B. C., Zhang, Q., Leitherer, C., et al. 1999, *AJ*, **118**, 1551
- Willick, J. A., Courteau, S., Faber, S. M., et al. 1997, *ApJS*, **109**, 333
- Zhang, Y., Gu, Q.-S., & Ho, L. C. 2008, *A&A*, **487**, 177